Subsynoptic-Scale Structure in a Major Synoptic-Scale Cyclone

CHRIS O'HANDLEY AND LANCE F. BOSART

Department of Atmospheric Science, State University of New York at Albany, Albany, New York

(Manuscript received 14 March 1988, in final form 23 September 1988)

ABSTRACT

An analysis of a major cyclone over the eastern United States in late February 1984 revealed the presence of several embedded well-defined mesoscale structures, including a low-level jet, a long-lived snowband and a strong upper-level front. Understanding the importance of these mesoscale features to the evolution of the synoptic-scale cyclone is the basis for this paper.

Evidence is presented that a period of weakening after initial surface cyclogenesis was the result of decoupling of the upper-level trough from the surface cyclone, as a consequence of the development of peripheral mesoscale precipitation systems. Redevelopment on the western side of the Appalachians occurred where orographic subsidence was amplified by a strong mesoscale low-level jet. Further intensification then took place when a strong upper-level frontal zone approached the surface cyclone. An incidental finding is that one of the mesoscale precipitation systems was a snowband, driven by strong synoptic-scale frontogenetical forcing rather than being a spontaneous consequence of conditional symmetric instability.

1. Introduction

A major cyclone affected most of the eastern half of the United States in late February 1984. This cyclone, whose track and intensity are summarized in Fig. 1, was not unusual in terms of intensity, size, or deepening rate. In fact, it was rather typical of fairly intense cyclones in that it exhibited a strong warm-sector squall line, a warm frontogenetical precipitation band, a low-level jet and a strong upper-level frontal zone, though it must be admitted that it is not clear how common the latter is. The review articles by Hane (1986), Keyser (1986) and Keyser and Shapiro (1986) discuss much of the previous research on these mesoscale features, which are common and have been thoroughly documented. Our goal in this paper, however, is to discuss how these various mesoscale features interact with each other and the synoptic-scale forcing, and the resulting effect on the evolution of the surface cyclone.

We performed an in-depth analysis of the cyclone structure at 1200 UTC 27 and 0000 UTC 28 February (Fig. 1). During this time, after an initial period of deepening, the surface cyclone became decoupled from its sustaining upper-level trough. Until a second period of deepening began at 0600 UTC 28 February, the central part of the cyclone was very unorganized, exhibiting multiple centers and continuously redeveloping northeastward toward the Appalachian Mountains. We feel that the 12 h period ending 0000 UTC 28 February, representative of the only really atypical aspect of the cyclogenesis, deserves study to determine the causes of the decoupling, disorganization and subsequent reintensification of the cyclone; this is the basis for most of the results presented.

The paper is organized as follows: Section 2 presents a synoptic overview, followed in section 3 by the kinematic vertical motion, frontogenesis and quasi-geostrophic forcing fields on selected pressure surfaces. The three-dimensional kinematic and thermodynamic structure of the atmosphere is examined in detail in section 4, while section 5 presents results of a moist potential vorticity analysis. This is followed by the discussion and concluding summary in sections 6 and 7.

2. Synoptic overview

a. Large-scale analysis

Figures 2 through 4 document the large-scale environment at the surface, and in the lower and upper troposphere, during the 48-hour period beginning 0000 UTC 27 February 1984. Prior to this time, a lee cyclogenesis event occurred over northeastern New Mexico as a deepening 500 mb trough crossed the southern Rockies. The cyclone intensified rapidly while moving away from the mountains, reaching 994 mb over northern Texas by 1200 UTC 26 February (Fig. 1). Precipitation coverage and intensity increased rapidly during this time, and a pre-cold frontal squall line began to form over eastern Texas.

By 0000 UTC 27 February (Fig. 2a) the cyclone has weakened, as evidenced by a 2 mb rise in the central pressure and a decrease of the pressure gradient near

Corresponding author address: Prof. Lance F. Bosart, Dept. of Atmospheric Science, Earth Science 219, State University of New York at Albany, Albany, NY 12222.

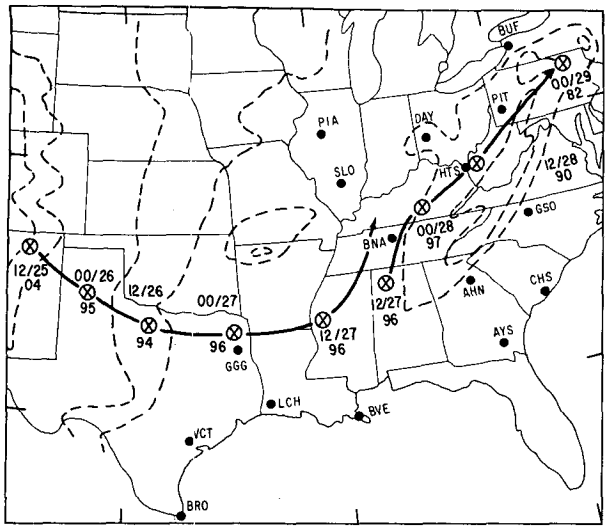

FIG. 1. Track of cyclone and central pressure (mb, leading 9 or 10 omitted) at 12-h intervals for the 84-hour period ending 0000 UTC 29 February 1984. Dashed lines indicate surface elevation above sea level (approximately 300, 600, 1500 and 2100 m). Locations of stations mentioned in text are indicated by solid dots with appropriate three letter identifier.

the storm center. Although the large-scale cyclonic circulation slowly increases, the cyclone center itself remains disorganized as it tracks eastward across the Gulf states, with two distinct circulation centers present at 1200 UTC 27 February. During this 12-hour interval the squall line attains peak intensity. Meanwhile, the anticyclone building into New England has established a northeasterly flow of cold dry air over the mid-Atlantic states, resulting in the development of cold air damming east of the Appalachians (Richwein 1980; Forbes et al. 1987; Bell and Bosart 1988) and coastal frontogenesis (Bosart 1975) just offshore. During the ensuing 12 hours the cyclone redevelops northeastward into Kentucky, with little change in strength. By 1200 UTC 28 February, however, significant deepening has occurred as the cyclone tracks northeastward along the western slopes of the Appalachians, while a weaker secondary development has taken place along the coastal front to the east.

The 850 mb cyclone (Fig. 3) undergoes a life cycle similar to that of the surface storm. It weakens slightly while moving eastward during the first 12 hours, then turns northeastward by 0000 UTC 28 February. During the final 12 hours, the circulation intensifies and moves almost due east to a position just west of the Appalachians. The analyses also reveal the presence of a strong low-level jet (LLJ) to the east-southeast of the cyclone during the entire period, but especially at 0000 and 1200 UTC 27 February. At these times the axis of the LLJ, which is associated with strong warm air and moisture advection, coincides very well with the observed precipitation pattern (refer to Fig. 2). Although this relationship becomes blurred after 1200 UTC 27 February, the weakening LLJ continues to be associated with strong warm air advection. Note that after 1200 UTC 27 February the thermal gradient northeast of the cyclone increases considerably, implying that strong frontogenesis is occurring there.

The upper tropospheric structure is portrayed by the $\theta = 320$ K isentropic analysis in Fig. 4. This level was chosen because it most clearly displays the structure of the upper tropospheric jet streams during the period of interest. A deepening large amplitude trough moves slowly eastward across the central United States while a strong jet streak propagates northeastward from the base of this trough. Comparison with Fig. 3 reveals that the exit region of this jet streak overlies the 850 mb LLJ during the first three periods. This observation, along with the fact that the LLJ first formed as the upper-jet exit region crossed the Rockies, suggests that the LLJ is dynamically coupled to the upper-level jet, as discussed by Uccellini and Johnson (1979).

Figure 4 also shows the location of the 500 mb vorticity maximum, determined from LFM (Limited-area Fine Mesh) model (Gerrity 1977) initial analyses, that was associated with the short-wave trough responsible for the original lee cyclogenesis event. At 0000 UTC 27 February the surface storm is under strong cyclonic vorticity advection (CVA). Nevertheless, the cyclone does not intensify, and by 1200 UTC 27 February the vorticity maximum has overtaken the surface cyclone, with the strong CVA moving to the north. Some kind of vertical decoupling process is apparently taking place (CVA is disrupted by mesoscale precipitation systems; to be discussed more fully in section 6b), resulting in the midtropospheric short-wave trough "outrunning" the surface cyclone. By 0000 UTC 28 February the decoupling process is complete, with the vorticity maximum over Illinois and the surface cyclone over southeastern Kentucky.

One other relevant feature is a strong upper level front (ULF) that developed in the northwesterly flow over the Rockies and propagated through the large scale trough. This front was best defined at 500 mb, and its position, based upon the 500 mb thermal gradient, is outlined on the surface maps in Fig. 2. The rapid deepening phase of the cyclone began when the downstream end of the ULF reached the vicinity of the cyclone center, suggesting that CVA associated with the ULF may have played a role in the observed deepening. The structure of this front, as well as its implications for surface development, is discussed in more detail in sections 4 and 6.

b. Subsynoptic scale analysis

In this section we examine in detail the observed surface conditions while the cyclone redevelops toward the Appalachian Mountains, through the use of surface sectional maps (Fig. 5) and 6 hour precipitation analyses (Fig. 6). Figure 5 reveals that there is a wedge of

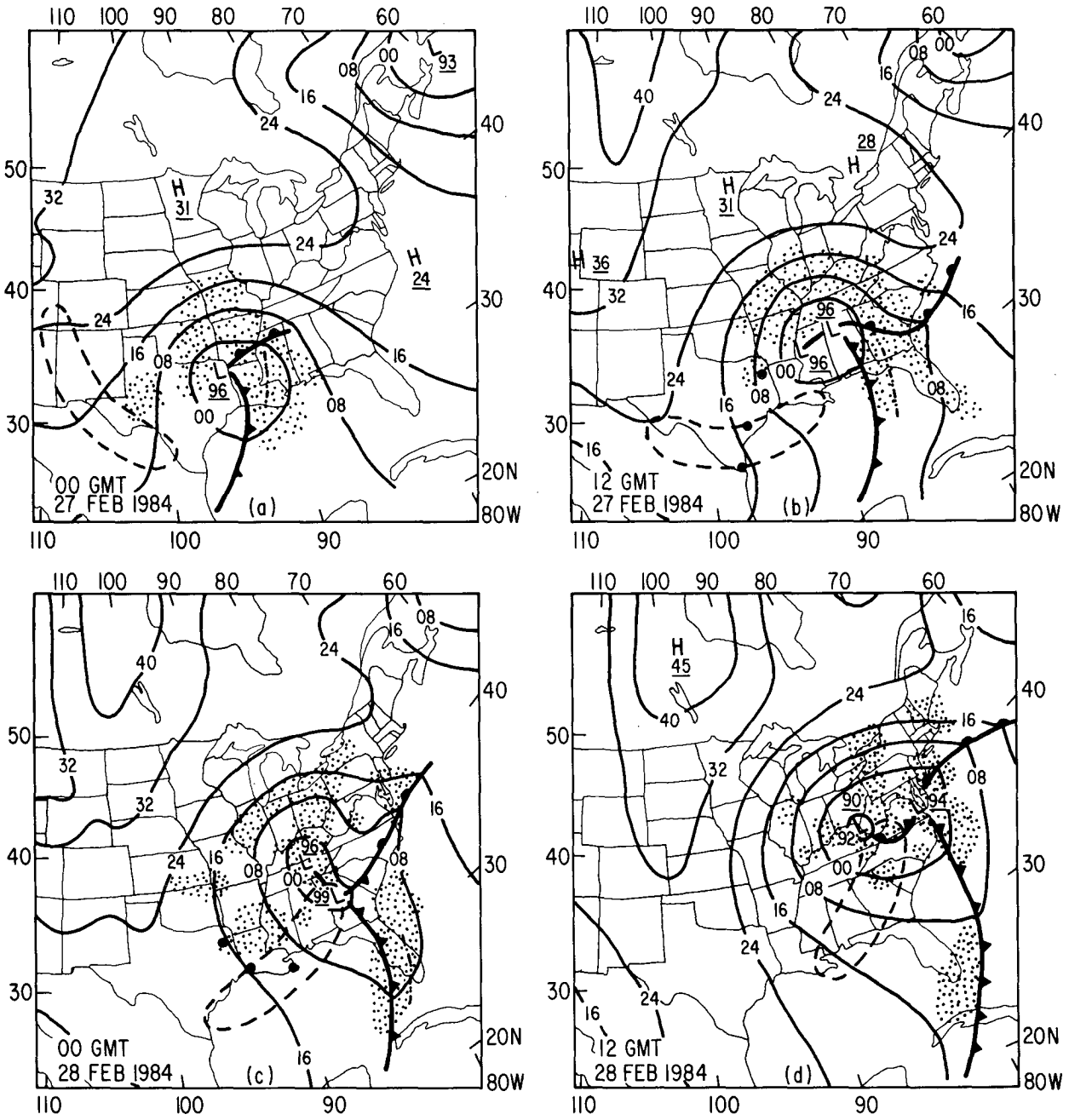

FIG. 2. Sea-level pressure (mb) and surface frontal analyses for 0000 UTC 27 February 1984 through 1200 UTC 28 February 1984. Stippling represents precipitation, with heavy dot-dashed line indicating position of a squall line. Location of 500 mb frontal zone, defined as the elongated region where the horizontal temperature gradient exceeds 2.5°C (100 km)$^{-1}$, is indicated by heavy dashed line. Heavy dots on panels (b) and (c) indicate locations of soundings shown on Fig. 9.

warm air nestled up against the west side of the Appalachians during the entire period from 1200 UTC 27 through 1200 UTC 28 February. The presence of strong easterly wind components at stations in this area suggests that adiabatic warming in downslope flow may be producing the local temperature maximum. Further evidence for this is the presence of a localized region of breaks in the low-level cloud cover early in the period over parts of eastern Kentucky and Tennessee. This shows up as a report of broken clouds in southeastern Kentucky in Fig. 5b, but is more clearly evident from visible satellite imagery (not shown). The resulting increased insolation enhances the warm wedge and also acts to destabilize the atmosphere locally.

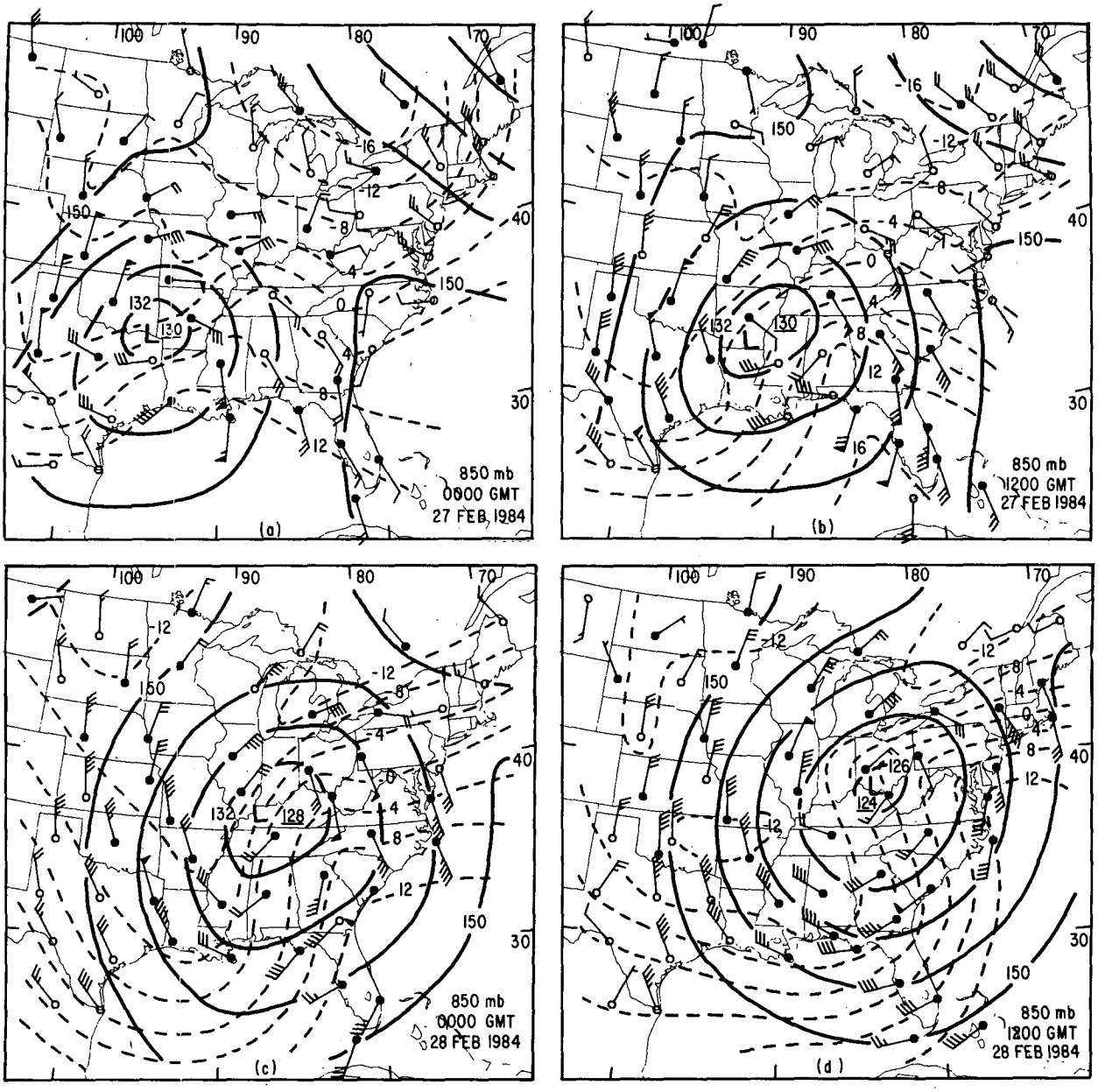

FIG. 3. The 850 mb height (interval 6 dam, solid), temperature (interval 4°C, dashed) and wind for 0000 UTC 27 February 1984 through 1200 UTC 28 February 1984. Solid circles indicate a dewpoint depression ≤ 5°C. One pennant, full barb and half barb represent 25, 5 and 2.5 m s^{-1}, respectively.

The sea-level pressure analysis reveals that the cyclone "center" is very disorganized throughout the period, being characterized by a flat pressure field with several embedded circulation centers. The original centers at 1200 UTC 27 February (Fig. 5a) move north-northeastward, weaken and eventually merge over northern Tennessee (Fig. 5a–d) while a new center forms in the warm air wedge over extreme eastern Tennessee (Fig. 5b). This center becomes dominant for about 6 hours (Fig. 5c–d), then weakens as well. Around 0600 UTC 28 February (Fig. 5g) yet another circulation center develops in the residual warm pocket near the Kentucky/West Virginia border. This center begins deepening, and by 1200 UTC 28 February (Fig. 5h) the cyclone has consolidated into a single-centered storm with a central pressure of 990 mb. Subsequently the cyclone moves northeastward along the western side of the Appalachians, deepening another 8 mb in the next 12 hours. Thus, after undergoing no significant intensity change for over 36 hours, the central pressure falls 14 mb in 18 hours. Meanwhile, a modest secondary circulation forms and moves northeastward along

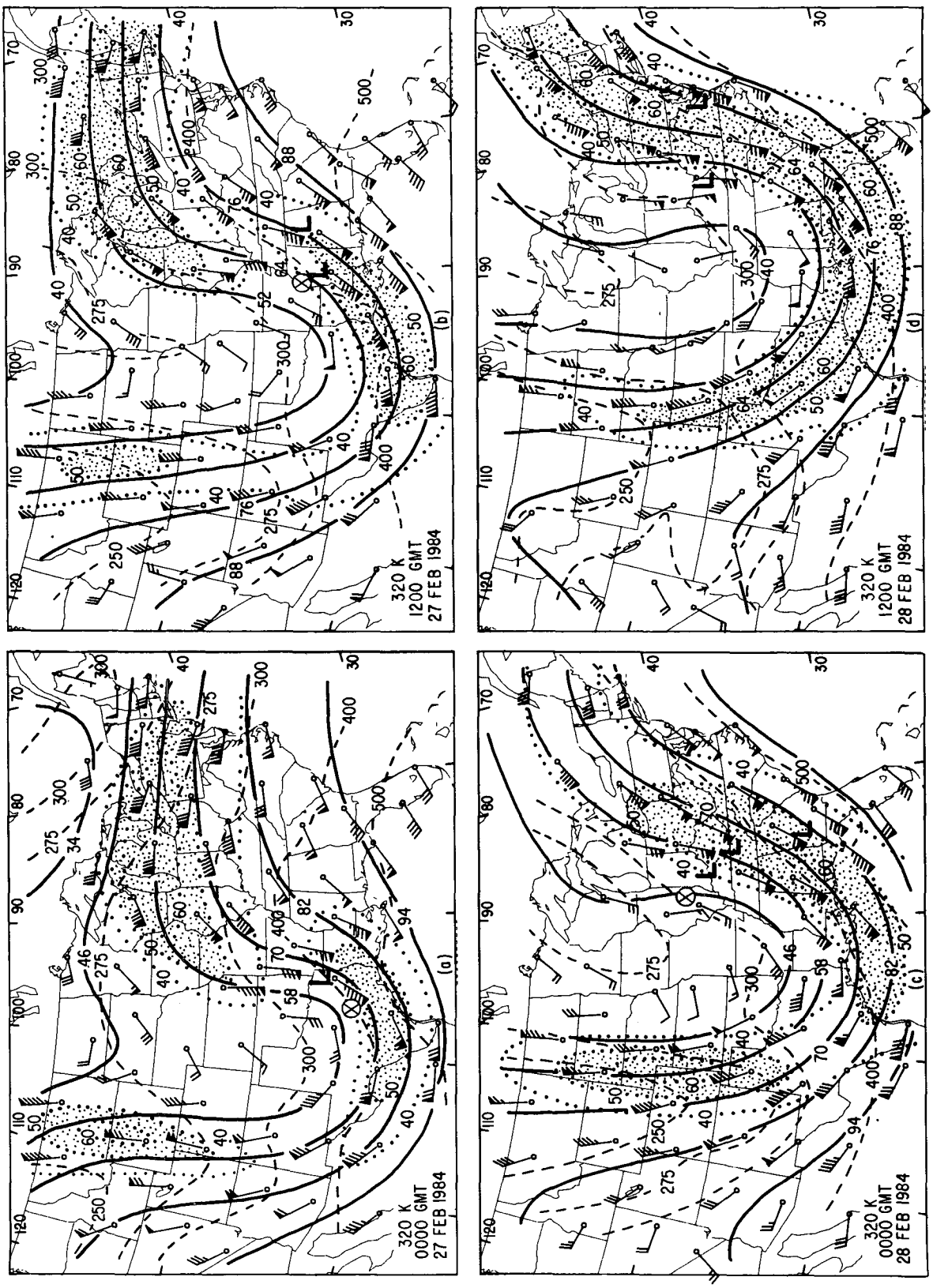

FIG. 4. Isentropic analysis on the $\theta = 320$ K surface for 0000 UTC 27 February 1984 through 1200 UTC 28 February 1984. Montgomery streamfunction (ψ_M) (solid, 58 = 3158 $\times 10^2$ m^2 s^{-2}), isobars [dashed, every 100 mb (25 mb) for pressure > 300 mb (<300 mb)] and isotachs (heavy dotted, m s^{-1}). Stippling represents areas where wind speed is >50 m s^{-1}. Wind barbs as in Fig. 3. Surface low positions indicated by heavy L's. On (a) through (c), circled x represents the location of the 500 mb vorticity maximum associated with the original cyclogenesis.

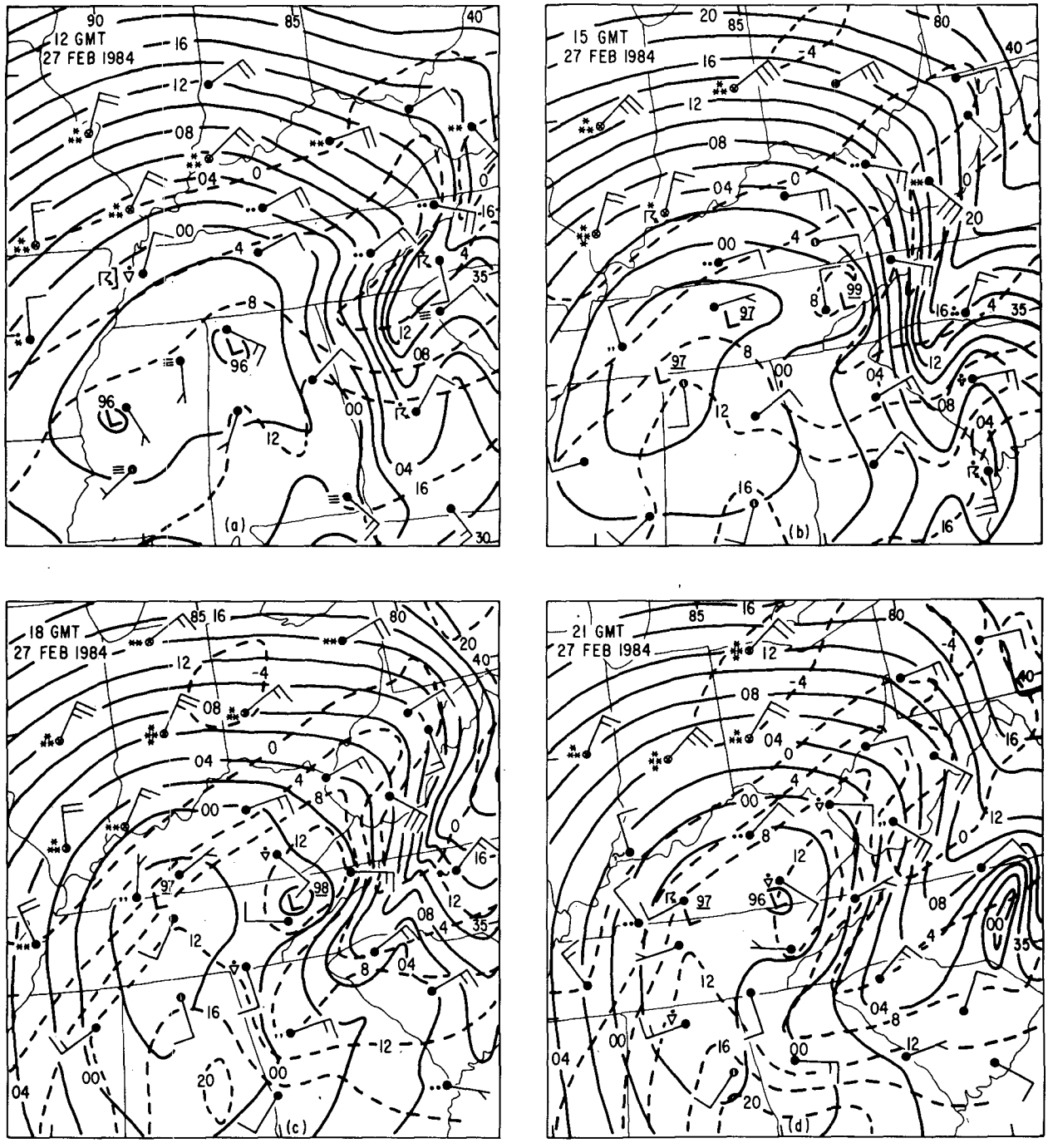

FIG. 5. Surface sectional analyses for 1200 UTC 27 February 1984 through 1200 UTC 28 February 1984. Sea-level pressure (solid) every 2 mb, isotherms (dashed) every 4°C. Conventional plotting notation for sky condition and current weather. Winds as in Fig. 3.

the coastal front (Fig. 5h). This system, though later associated with locally heavy rainfall further north along the coast, never became the dominant circulation.

Figure 5 shows that during the early part of the period (Fig. 5a–c) precipitation is concentrated in two mesoscale systems, a squall line to the east-southeast of the cylone and a southwest–northeast oriented band of moderate to heavy snow to the north-northwest of the cyclone. Both are long-lived systems, with the squall line having moved eastward from Texas and the snowband having formed over Oklahoma and southwestern Missouri around 0000 UTC 27 February. The squall line moves quickly offshore and dissipates while in its

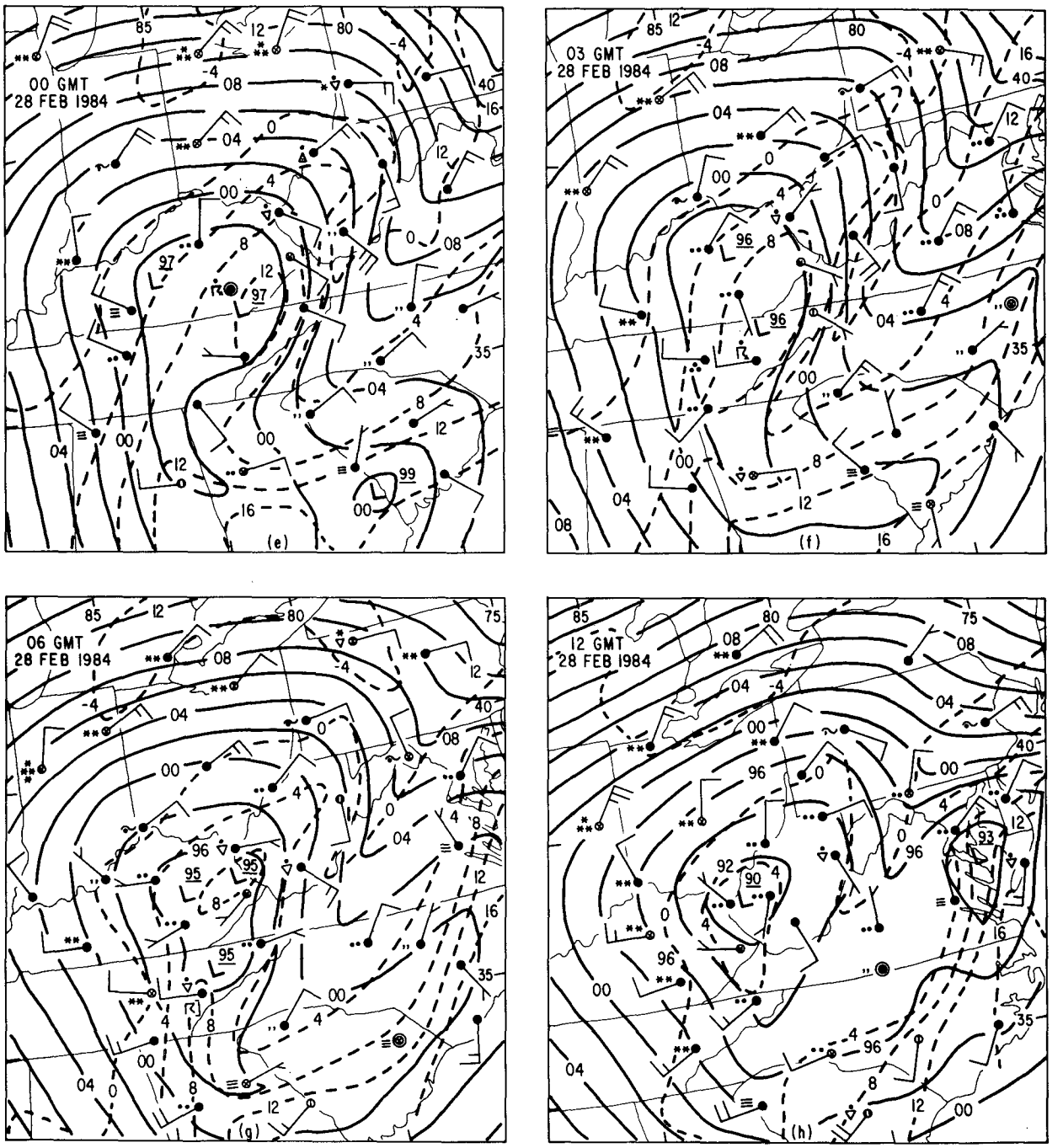

FIG. 5. (*Continued*)

wake a gravity wave (described more fully by Bosart and Seimon 1988) intensifies and moves eastward across the Carolinas (Figs. 5c–d). Meanwhile the snowband intensifies and moves steadily northeastward, leaving the region by 0300 UTC 28 February (Fig. 5f). However, the precipitation analysis (Fig. 6) shows that the snowband persists through at least 1200 UTC 28 February. The average length and width of the 10-mm isopleth in the band during the four periods is 400 km × 85 km. In addition, the average half-width (the lateral distance from the point of maximum precipitation to the point receiving half this amount) is also about 85 km. Thus, the width of the band is comparable to that of a snowband studied by Sanders and Bosart (1985) in an East Coast snowstorm. Note that the orientation of the band remains constant through-

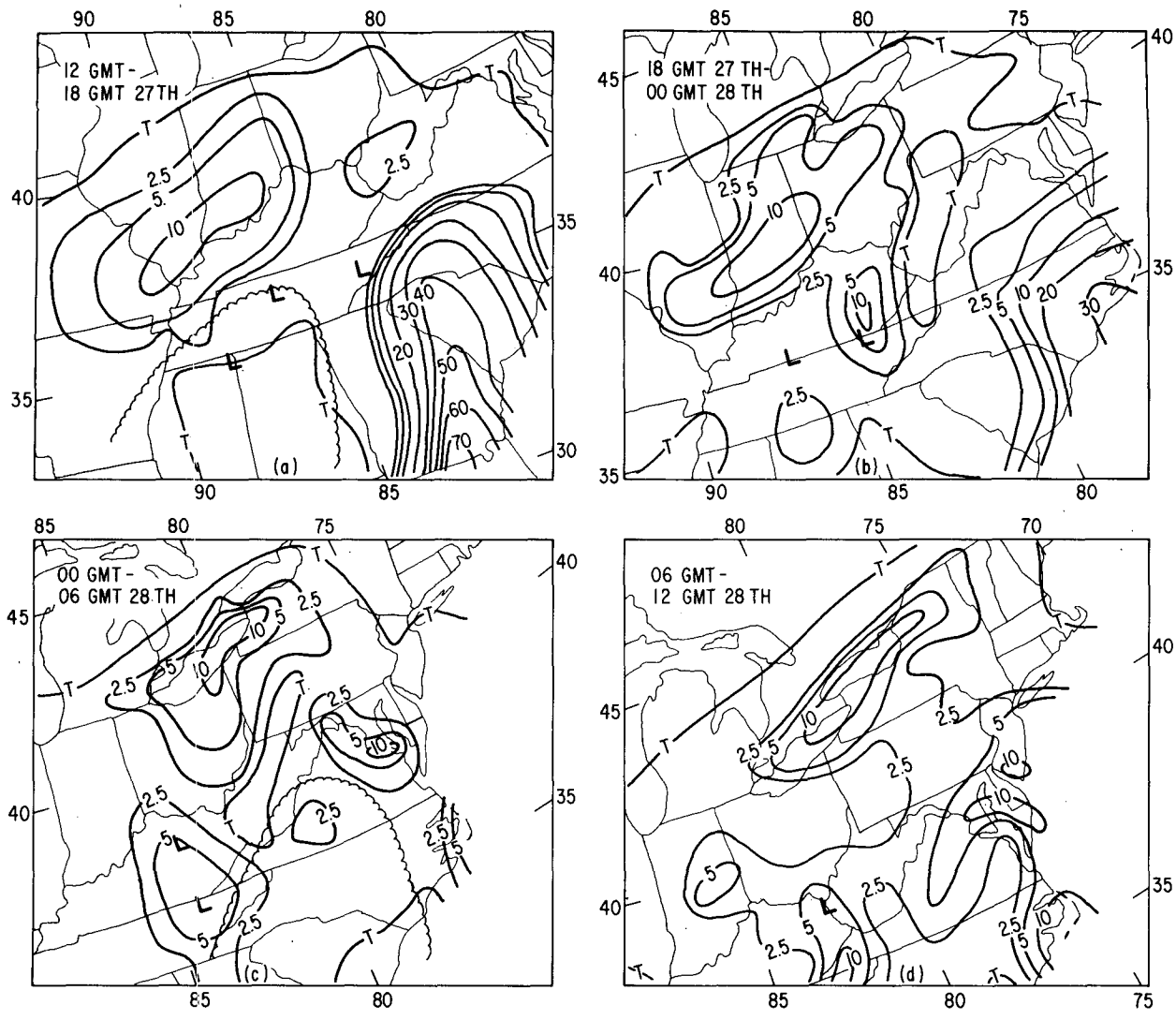

FIG. 6. Accumulated 6-h precipitation (mm) for 1200 UTC 27 February 1984 through 1200 UTC 28 February 1984. Surface low positions at the midpoint of each 6-h period are indicated by heavy L's. Scalloped line on (a) and (c) encloses region covered by low and mid-tropospheric dry intrusion.

out the period, and the band moves steadily northeastward, despite all the changes in motion of the surface cyclone.

Several other interesting features are revealed by the precipitation analysis. Initially, there is only very light precipitation in the vicinity of the cyclone center (Figs. 6a and 5a–c). However, there is a considerable increase in the coverage and intensity of precipitation, including widespread convective activity, near the cyclone center just before the onset of the final period of deepening (Figs. 6b–c and 5d–g). In particular, thunderstorms developed over west-central Kentucky at 2100 UTC 27 February and moved into the eastern parts of Kentucky and Tennessee by 0000 and 0300 UTC 28 February. This convective development, in which radar-derived echo tops were approximately 6.5 km, is more clearly seen from satellite imagery (not shown). Finally, Fig. 6 reveals that a narrow, northeastward-moving precipitation-free zone exists along the western slopes of the Appalachians during the second and third periods. An explanation could focus on the presence of a deep dry intrusion approaching from the southwest above 800 mb, the position of which is marked on Figs. 6a and 6c for 1200 UTC 27 and 0000 UTC 28 February. However, the scale of this feature greatly exceeds that of the surface dry zone. In addition, other areas under the dry intrusion received measureable precipitation. It seems more likely that this dry zone represents a rain shadow effect due to locally enhanced subsidence west of the mountains.

3. Vertical motion and frontogenesis

In this section we examine the kinematically computed vertical motion field at two levels, 800 and 500

mb, and compare the results with a quasi-geostrophic (QG) diagnosis. These computations, and those to follow, are based on a subjectively analyzed dataset of geopotential, temperature, dewpoint and observed winds for nine pressure levels at 100 mb intervals from the surface (1000 mb) to 200 mb. The analysis of tight gradients of temperature, dewpoint and windspeed was aided by the use of cross sections and individual soundings. The data were tabulated on a 1° latitude–longitude grid over a 25° × 30° region approximately centered on the cyclone. This procedure was performed for both 1200 UTC 27 February and 0000 UTC 28 February.

The kinematic computation is made using an orographic contribution, defined by $\omega_T = -\rho g(\mathbf{V}\cdot\nabla z)$ as the bottom boundary condition at 1000 mb (Dallavalle and Bosart 1975). At 200 mb the vertical motion is forced to zero by the O'Brien (1970) linear correction scheme, in which the adjustment to ω and $\nabla\cdot\mathbf{V}$ increases upward. This method was chosen because of the presence of an increasing number of questionable and missing wind reports above jet stream level, especially at 300 and 200 mb. The QG forcing of vertical motion was evaluated using the **Q**-vector method of Hoskins et al. (1978) and Hoskins and Pedder (1980). Briefly,

$$\mathbf{Q} = \left(-\frac{\partial \mathbf{V}_g}{\partial x}\cdot\nabla\theta, -\frac{\partial \mathbf{V}_g}{\partial y}\cdot\nabla\theta\right) \tag{1}$$

and the QG vertical velocity can be determined, ignoring the beta effect, from

$$\sigma\nabla^2\omega + f_0{}^2\frac{\partial^2\omega}{\partial p^2} = -2\nabla\cdot\mathbf{Q}. \tag{2}$$

The static stability, σ, is given by

$$\sigma = -\frac{R}{P}\left(\frac{p}{p_0}\right)^{\kappa}\frac{\partial\theta}{\partial p}, \tag{3}$$

where θ is the potential temperature, $\kappa = R/c_p$, $p_0 = 1000$ mb and the other symbols have their usual meteorological meaning. Equation (2) was not solved for ω, but instead the field of $\nabla\cdot\mathbf{Q}$ was used to examine the QG forcing, with convergence (divergence) of the **Q**-vectors implying ascent (descent). As pointed out by Durran and Snellman (1987), however, if (2) is solved for ω, it is possible that at a given level the forcing term will not be in phase with the actual value of ω. In general, the approximation works best in the midtroposphere. Finally, since **Q** is equal to the rate of change of the potential temperature gradient moving with the horizontal geostrophic velocity, it follows that

$$\frac{d}{dt}|\nabla\theta| = \frac{1}{|\nabla\theta|}\mathbf{Q}\cdot\nabla\theta \tag{4}$$

is a measure of geostrophic frontogenesis. Thus, in regions where the **Q**-vectors are oriented toward higher (lower) θ, there is QG frontogenesis (frontolysis). For comparison, observed wind frontogenesis was computed from the two-dimensional adiabatic version of Miller's (1948) equation, which is

$$\frac{d}{dt}|\nabla\theta| = \frac{1}{|\nabla\theta|}\left\{\frac{\partial\theta}{\partial x}\left[-\frac{\partial u}{\partial x}\frac{\partial\theta}{\partial x} - \frac{\partial v}{\partial x}\frac{\partial\theta}{\partial y}\right] + \frac{\partial\theta}{\partial y}\left[-\frac{\partial u}{\partial y}\frac{\partial\theta}{\partial x} - \frac{\partial v}{\partial y}\frac{\partial\theta}{\partial y}\right] + \frac{\partial\theta}{\partial p}\left[-\frac{\partial\omega}{\partial x}\frac{\partial\theta}{\partial x} - \frac{\partial\omega}{\partial y}\frac{\partial\theta}{\partial y}\right]\right\}. \tag{5}$$

In subsequent discussions, observed frontogenesis refers to the combination of the first two sets of bracketed terms, which include the effects of horizontal shear and confluence, in order to facilitate direct comparison with the **Q**-vector form. The twisting terms, in the third set of brackets, are discussed separately where appropriate.

The kinematic results are presented in Fig. 7, and the corresponding QG analyses are in Fig. 8. At 1200 UTC 27 February the 800 mb kinematic analysis reveals a band of strong ascent that curves cyclonically about the storm center. The strongest ascent, -15×10^{-3} mb s^{-1}, is associated with the LLJ/squall line over western Georgia, and strong ascent extends to over the surface snowband. Moderate descent is occurring in the cold advection area over Texas, with an eastward extension along the Gulf coast. This extension, which curves northward toward the cyclone, is associated with the dry intrusion that extends to over south central Tennessee above 800 mb. A similar pattern is observed at 500 mb, with maximum ascent of -23×10^{-3} mb s^{-1} over southeastern Tennessee. The ascent region over the Mississippi Valley slopes northward with height, consistent with the presence of large-scale slantwise ascent. In addition, the region near the snowband exhibits a lower tropospheric ascent maximum, which ranges from 800 mb on the southern side to 700 mb on the northern side of the band. Meanwhile, the ascent area farther southeast displays little slope with height, as would be expected in a region of vigorous buoyant convection. The ascent within the squall line maximizes in the 600–700 mb layer.

The QG analysis at 1200 UTC 27 February (Fig. 8a, b) reveals strong forcing of ascent at 800 mb along the LLJ (compare with Fig. 3b), and less pronounced forcing at 500 mb in the same region. This is consistent with the presence of a local maximum of lower tropospheric warm advection along the jet, which maximizes over Kentucky and Tennessee. Examination of the **Q**-vectors (and computations, not shown) reveals considerable QG frontogenesis along the LLJ, particularly near its northern terminus over the Ohio Valley, with a maximum of 1.4°C (100 km)$^{-1}$ (3 h)$^{-1}$ over southeastern Indiana. This agrees well with the observed wind frontogenesis (not shown), which exhibits a similar pattern and a maximum of 1.7°C (100 km)$^{-1}$ (3 h)$^{-1}$ over southwestern Indiana. Due to the strong kinematically computed vertical motion gra-

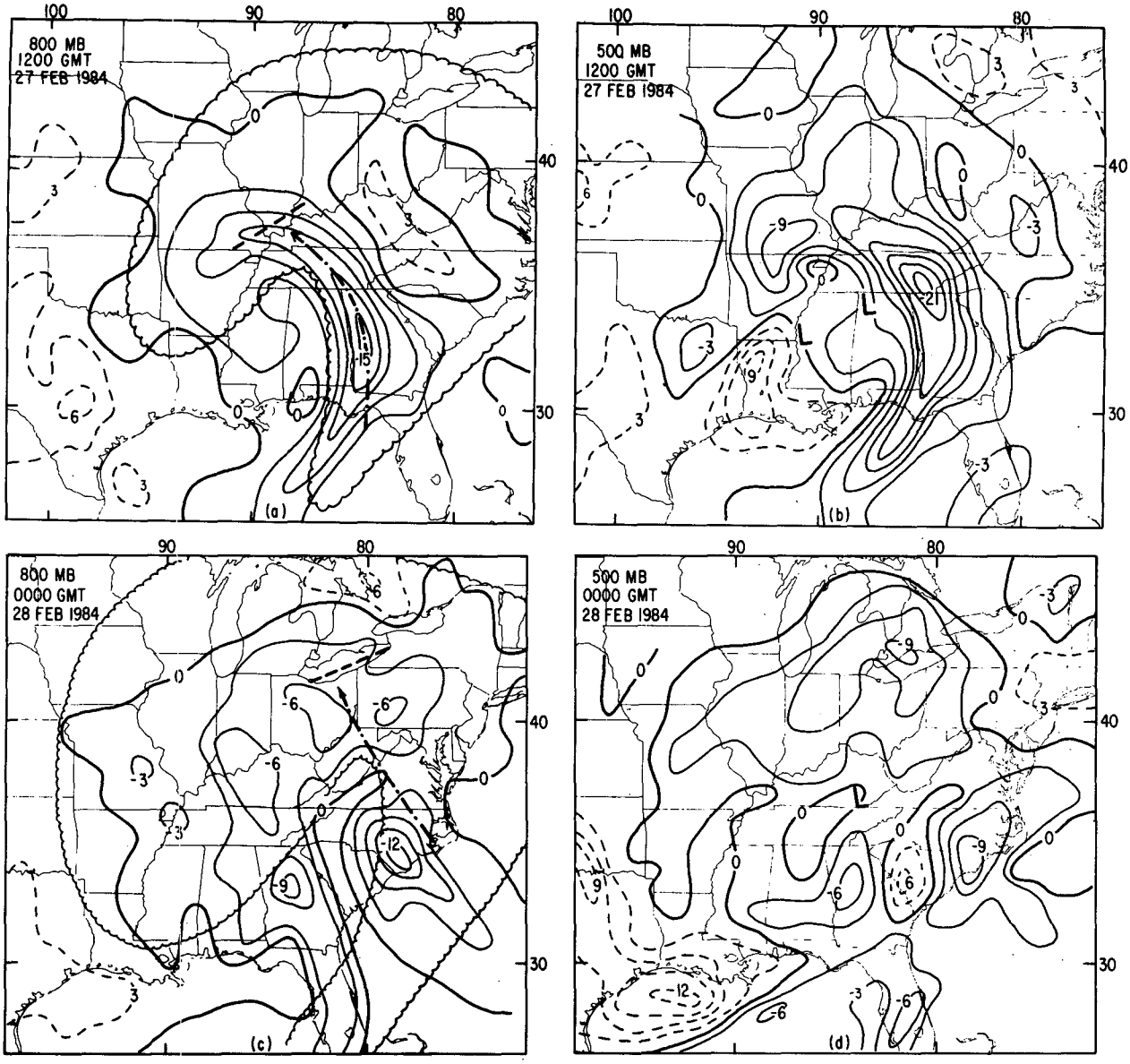

FIG. 7. The 800 and 500 mb kinematic vertical motions for 1200 UTC 27 February and 0000 UTC 28 February 1984. Zero vertical motion, ascent and descent are indicated by heavy solid, thin solid and thin dashed lines, respectively. Contour interval is 3×10^{-3} mb s^{-1}. On panel (a) and (c), scalloped line encloses major cloud mass, heavy dashed line is snowband axis and heavy dot-dashed line represents axis of low-level jet at 800 mb. Locations of surface cyclone centers indicated on panels (b) and (d).

dients near the jet and snowband, the twisting contribution to frontogenesis is very large. It is negative at all levels and increases upward, reaching a maximum at progressively higher levels northward along the jet. At 900 mb there is a small [1 °C (100 km)$^{-1}$ (3 h)$^{-1}$] positive total frontogenetic tendency along the entire jet. By 800 mb the LLJ is dominated by negative total frontogenesis, though there is still a small region of positive total frontogenesis along the snowband. At and above 700 mb, however, twisting dominates the entire region, resulting in negative total frontogenesis. This picture is consistent with previous results (i.e., Sanders 1955) concerning the upward increase in importance of twisting as a frontolytic mechanism in strong lower tropospheric baroclinic zones.

At 500 mb, very strong forcing of ascent is present over southeastern Missouri, reflecting the vigor of the short-wave trough, which is becoming decoupled from the surface cyclone. Elsewhere, significant descent is implied over southern Texas in the region of strong frontogenesis [2°C (100 km)$^{-1}$ (3 h)$^{-1}$ from QG versus 1.4°C (100 km)$^{-1}$ (3 h)$^{-1}$ from observed winds] accompanying the upper-level frontal zone, while a band of forcing of ascent exists just to the east.

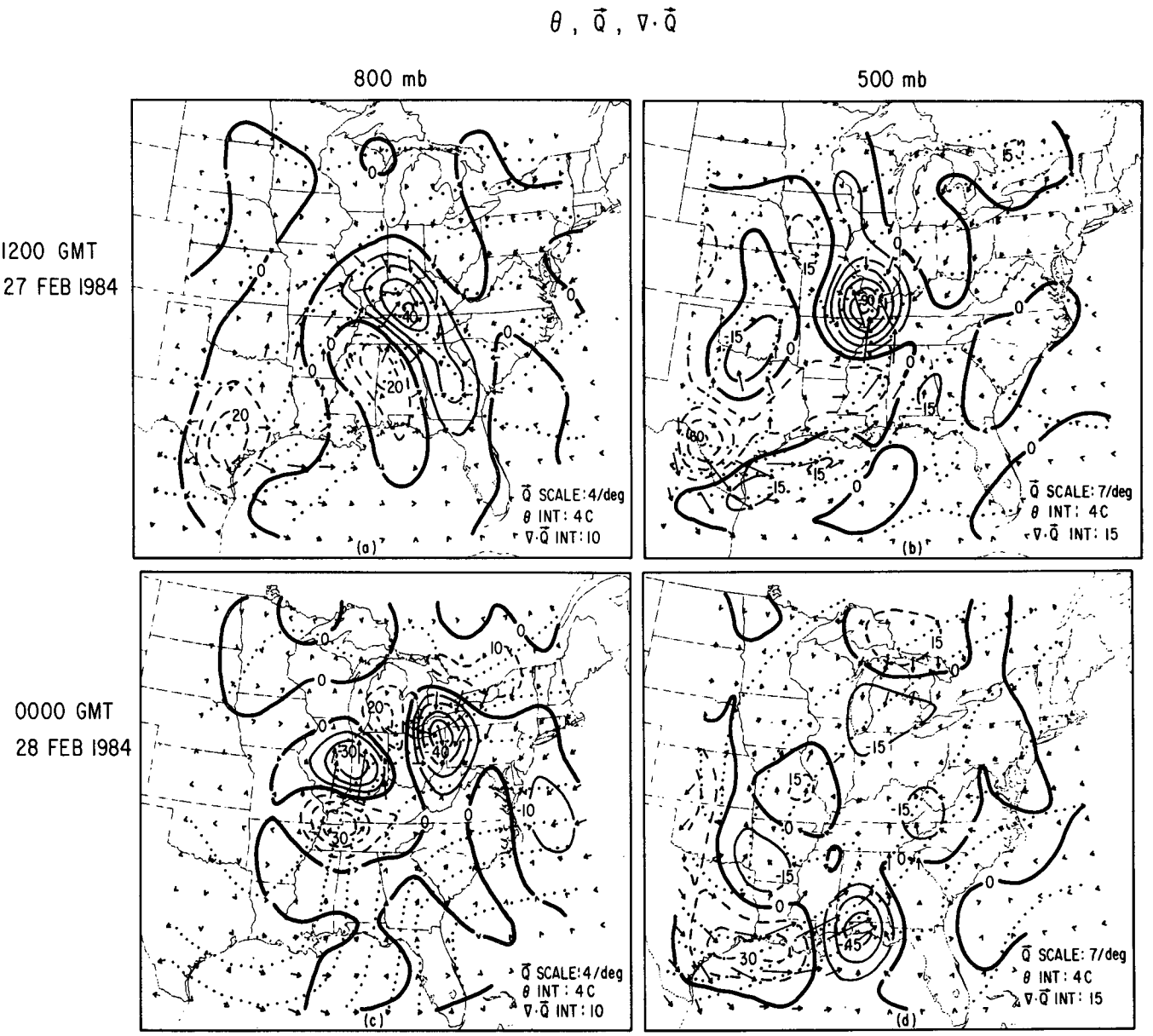

FIG. 8. Q-vectors (10^{-9} K s^{-1} m^{-1}), $\nabla \cdot \mathbf{Q}$ (10^{-16} mb^{-1} s^{-3}) and potential temperature (interval 4°C) at 800 and 500 mb for 1200 UTC 27 February and 0000 UTC 28 February 1984. Heavy solid line represents $\nabla \cdot \mathbf{Q} = 0$, thin solid (dashed) lines represent convergence (divergence) of **Q**. Note: **Q**-vectors are plotted every 2° of latitude–longitude.

At 0000 UTC 28 February the low-level kinematic vertical velocity field (Fig. 7c) is no longer dominated by a single cyclonically curved band of ascent. Instead, there is an ascent maximum located near the snowband over Ohio (again, the snowband ascent maximizes in the 800–700 mb layer), and a band of ascent extending from the cyclone center in Kentucky along the cold front into Florida. The separate ascent maximum over North Carolina may be associated with a coastal front circulation or perhaps with a large amplitude gravity wave, which is just moving offshore (Bosart and Seimon 1988). At 500 mb (Fig. 7d) strong ascent is diagnosed above the snowband, while weak descent is found directly above the surface cyclone. Further south, strong descent is suggested along the northwestern Gulf coast, in the entrance region of the upper level front (refer to Fig. 2c).

The corresponding QG analysis (Fig. 8c, d) reveals strong lower tropospheric forcing of ascent within the snowband, which coincides with an area of strong QG frontogenesis [maximum of 1.5°C (100 km)$^{-1}$ (3 h)$^{-1}$ just west of BUF]. Frontogenesis computations based on the observed winds are twice as large [up to 3°C (100 km)$^{-1}$ (3 h)$^{-1}$, though the patterns are iden-

tical], while the twisting term is operating in the same manner as 12 hours earlier. At 500 mb the forcing associated with the now weakened short wave trough is seen over the southern Great Lakes, while strong forcing of descent is found in the frontogenetic entrance region of the ULF. The maximum observed wind frontogenesis in the ULF is twice as large as that computed quasi-geostrophically [3.3 versus 1.6°C (100 km)$^{-1}$ (3 h^{-1})], though the patterns are identical. More importantly, however, the analysis reveals the presence of two local maxima of forcing of ascent over and upstream of the surface cyclone. The first, over eastern Kentucky, is quite weak but its arrival time closely coincides with the outbreak of convection observed near the cyclone center. The second, over southern Alabama, is considerably stronger, and appears to be associated with some weak kinematic ascent. Both maxima appear to have originated within the band of forcing in the western Gulf of Mexico 12 hours earlier (Fig. 8b). Extrapolating the second maximum forward yields an arrival time over the surface cyclone between 0600 and 0900 UTC 28 February, which coincides with the beginning of rapid surface deepening.

4. Detailed atmospheric structure

a. Upper troposphere

During the synoptic overview it was pointed out that an intense upper-level front (ULF) moved through the large-scale trough over the central United States. The intensity of this feature can be seen from the temperature and wind soundings taken at stations within the frontal region at 1200 UTC 27 February and 0000 UTC 28 February (Fig. 9; refer to Fig. 2 for location of these soundings relative to synoptic features). At both times the upper-level frontal layer is generally confined between $\theta = 303$ and 323 K. The base of the frontal layer penetrates to at least 660 mb (at BRO) at 1200 UTC 27 February. At 0000 UTC 28 February the maximum downward penetration is uncertain, as the southern boundary of the ULF is over the Gulf of Mexico. It appears that the strength of the frontal inversion has increased during the 12 hours, and this is supported by an increase in the 500 mb temperature gradient (not shown), consistent with the presence of strong QG and observed wind frontogenesis as discussed earlier.

Figures 10 and 11 present a 500 mb vorticity analysis for 1200 UTC 27 February and 0000 UTC 28 February, respectively. The analysis is based on the Eulerian vorticity equation, which is

$$\frac{\partial \zeta}{\partial t} = -\mathbf{V}\cdot\nabla(\zeta + f) - \omega\frac{\partial \zeta}{\partial p} - (\zeta + f)\nabla\cdot\mathbf{V} - \mathbf{k}\cdot\nabla\omega\times\frac{\partial \mathbf{V}}{\partial p}, \quad (6)$$

where ω is the kinematically computed vertical velocity. The terms on the right side of (6) (horizontal and vertical advection of absolute vorticity, vorticity production by convergence and the twisting term) are examined individually and then summed to yield an instantaneous local vorticity tendency. The most striking feature at 1200 UTC (Fig. 10a) is the cyclonic vorticity maximum of 29×10^{-5} s^{-1} located along the Arkansas/Mississippi border, north of the surface cyclone. This feature is associated with strong cyclonic vorticity advection (CVA) (Fig. 10b), which increases upward

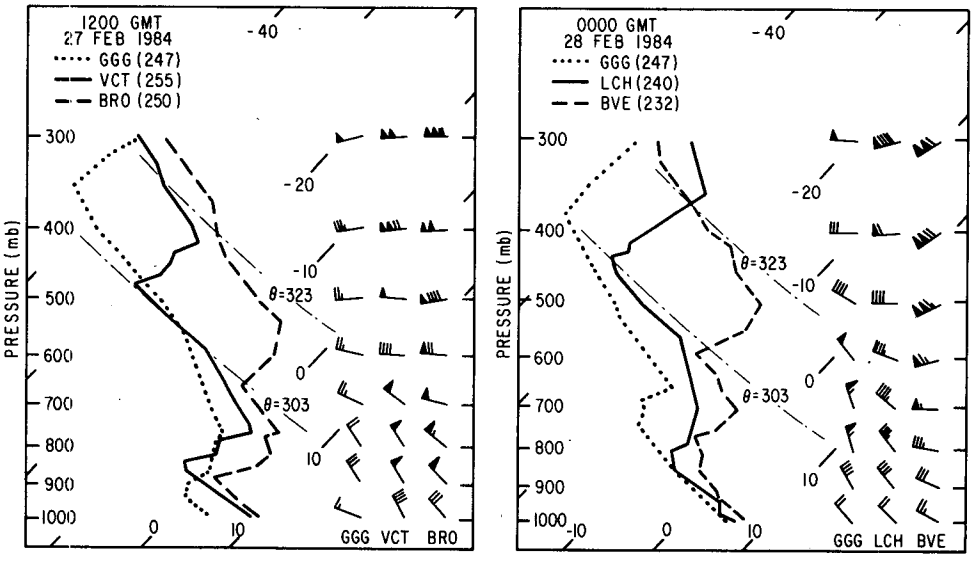

FIG. 9. Temperature soundings (skew T-log p format) across upper-level front at (a) 1200 UTC 27 February 1984 (b) 0000 UTC 28 February 1984. Plotted winds as in Fig. 3.

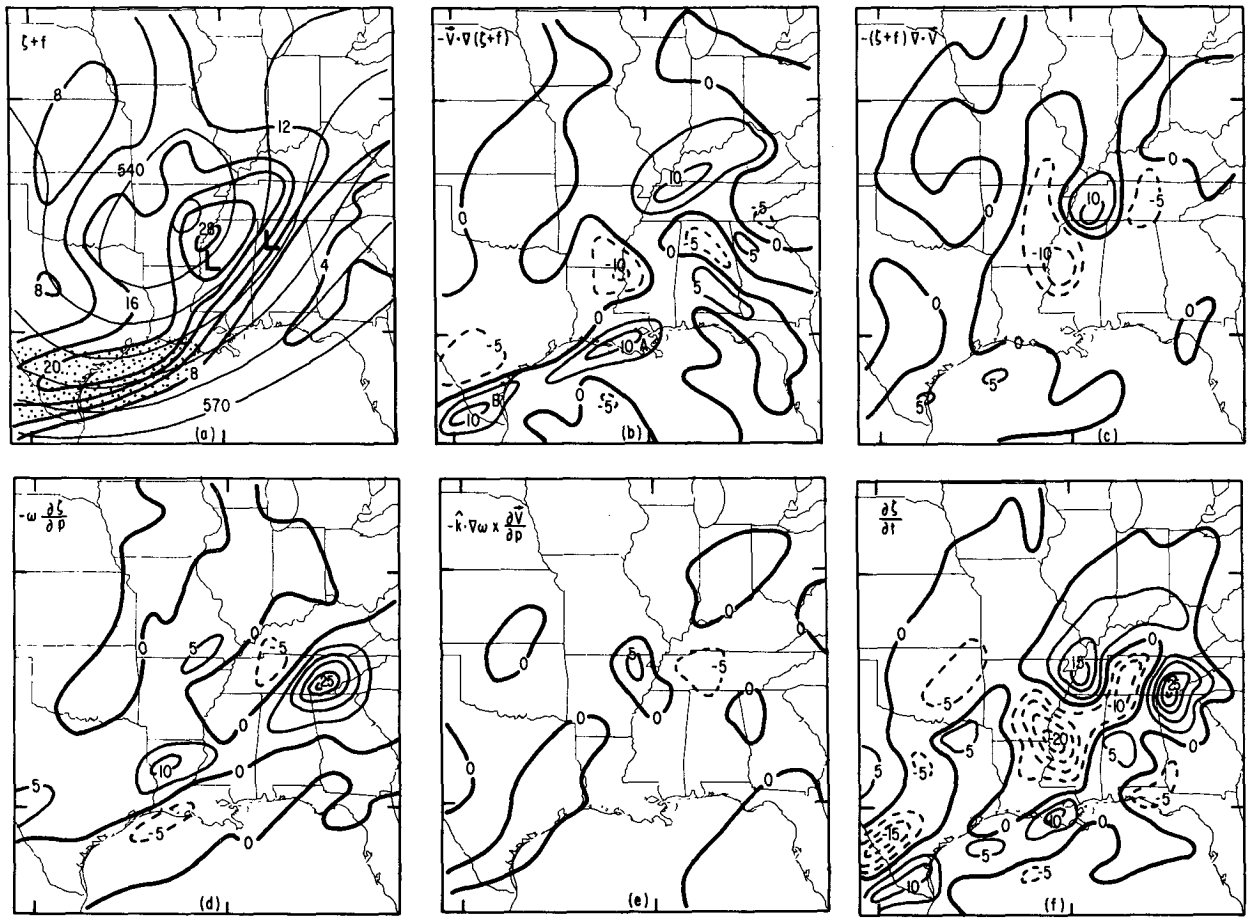

FIG. 10. The 500 mb vorticity analysis at 1200 UTC 27 February 1984. (a) 500 mb height (thin solid, interval 6 dam) and absolute vorticity (heavy solid, interval 4×10^{-5} s^{-1}). Stippled area represents region where the thermal gradient within the upper level front exceeds 2.5°C (100 km)$^{-1}$, and surface low positions are indicated by heavy L's. (b) Horizontal vorticity advection. (c) Convergence term. (d) Vertical vorticity advection. (e) Twisting term. (f) Total local vorticity tendency. On (b)–(f), zero contour is heavy solid with positive (negative) tendencies given by thin solid (dashed) lines, and contour interval is 5×10^{-9} s^{-2}.

from 600 to 400 mb, consistent with the QG diagnosis presented earlier (Fig. 8b). Comparison with the convergence term (Fig. 10c) reveals an in phase relationship between the two over western Tennessee, opposite to the relationship expected from QG theory. The remaining terms, vertical advection and twisting, are generally smaller but locally important. The resultant local vorticity tendency (Fig. 10f) shows a well-defined positive/negative couplet associated with the Arkansas short wave. The presence of negative tendencies at the vorticity maximum, however, indicates that the wave is weakening.

A second local maximum of vorticity is found along the Texas coast, within and to the cold side of the upper frontal zone. Considerable CVA is associated with this feature, with two local CVA maxima, labelled A and B, clearly evident. Reference to Fig. 8b reveals that these maxima are associated with a region of QG forcing on the warm side of the ULF. Examination of the remaining terms reveals that the dominant generating mechanism for new vorticity in the ULF is convergence, though the magnitude is not very large. However, the smallness of this term may be due to the lack of offshore data. At 400 mb (not shown), where the ULF is mainly over land, the convergence vorticity production covers a larger area and maximizes at 10 $\times 10^{-9}$ s^{-2}.

By 0000 UTC 28 February (Fig. 11a) the 500 mb vorticity pattern has changed considerably. The vorticity maximum originally over Arkansas has moved northward and weakened, and is no longer associated with any significant vorticity advection. However, there has been a dramatic increase of vorticity within the ULF zone, and this vorticity has been advected downstream in a narrow band that extends to just east of the surface cyclone. This band exhibits a width (distance across the 16×10^{-5} s^{-1} isopleth) of approximately 170 km over eastern Tennessee, just upstream of the surface low. Two local maxima of CVA along this band (Fig. 11b) seem to have continuity with CVA

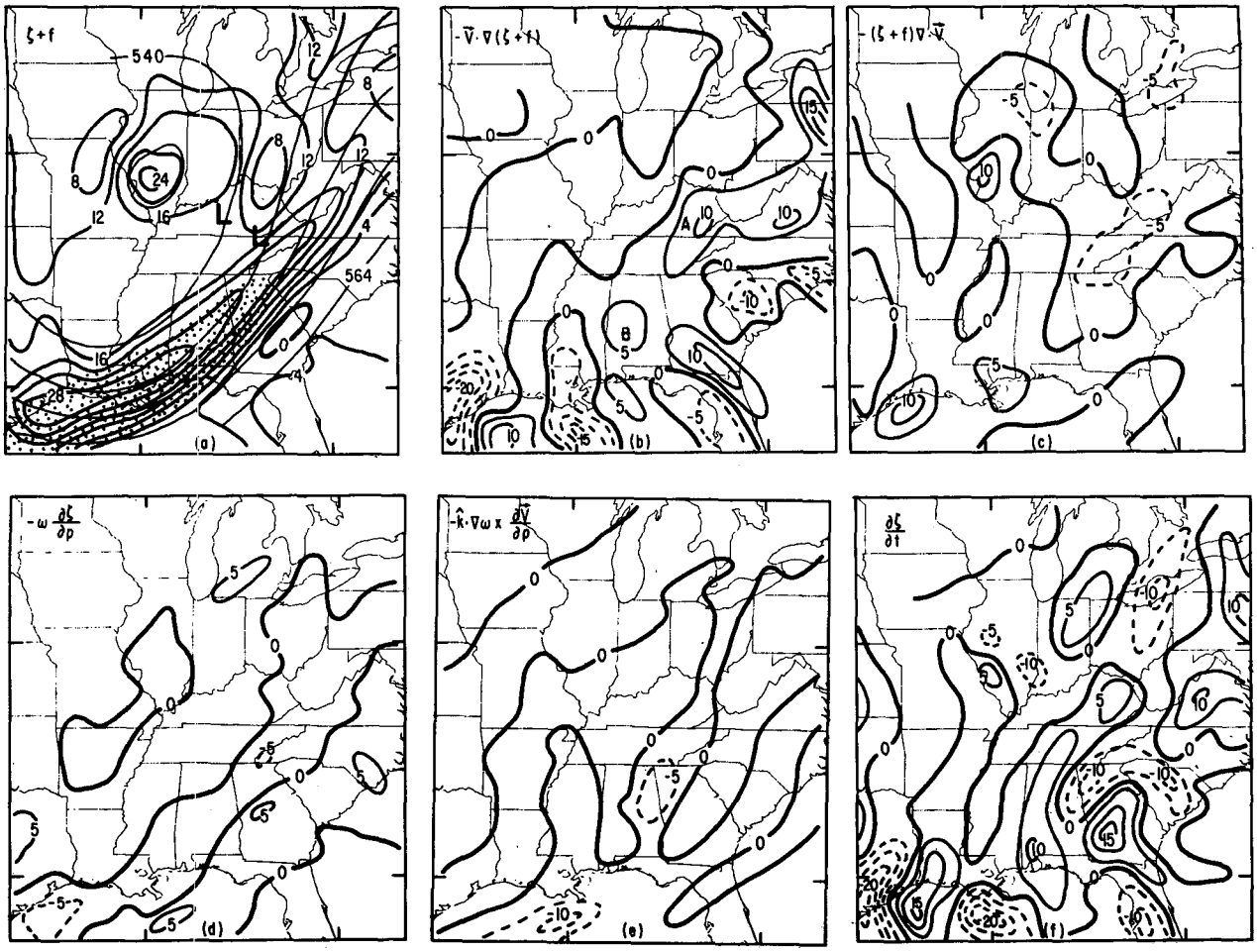

FIG. 11. As in Fig. 10 except for 0000 UTC 28 February 1984.

areas A and B that existed 12 hours earlier (Fig. 10b), implying a translational speed of 25 m s^{-1} to the northeast. Note that these maxima correspond with the areas of strong QG forcing seen earlier (Fig. 8d). Examination of the remaining terms reveals that convergence is the most important mechanism generating new vorticity within the entrance region of the ULF. The magnitude of this effect has increased since 1200 UTC 27 February (at 400 mb as well, not shown) as the ULF enters the confluent, frontogenetic southwesterly flow ahead of the trough axis.

In summary, the 500 mb vorticity analysis reveals that prior to rapid surface deepening, a strong ULF moves through the base of the 500 mb trough and enters the confluent southwesterly flow region. Strong vorticity production occurs, due mainly to convergence, and the resulting vorticity is advected downstream in a narrow band, toward the surface cyclone. Two distinct vorticity advection impulses are observed, with the first apparently aiding the development of convection near the cyclone center shortly before 0000 UTC 28 February. The extrapolated arrival time of the second, based on the 12-hour motion between 1200 UTC 27 February and 0000 UTC 28 February, coincides with the beginning of rapid surface deepening near HTS at 0600 UTC 28 February. The implications of these observations are discussed in section 6.

b. Lower troposphere

In this section we examine the kinematic and thermodynamic structure of the key lower tropospheric features, the LLJ and the snowband. An analysis of the θ_e = 308 K surface, chosen as being representative of the LLJ, is presented in Fig. 12. At 1200 UTC 27 February the LLJ is clearly defined as an anticyclonically curved, rapidly ascending airstream originating near the surface over central Georgia. The pressure maximum along the jet axis shows that the LLJ represents a θ_e maximum in the lower troposphere, indicating the importance of this feature as a source of warm, moisture-laden air for the cyclone. A crude estimate of the maximum ascent along the jet, from the method used by Carr and Millard (1985) except ig-

noring system translation, yields a value of -15×10^{-3} mb s^{-1} at 700 mb over western Kentucky, almost identical to the kinematically computed value of -13×10^{-3} mb s^{-1}. Although the jet axis passes just south of the Appalachian mountains, a 900 mb analysis (not shown) reveals that winds of 15–20 m s^{-1} do cross the high mountains along the Tennessee/North Carolina border. The flow is perpendicular to the topography, and it is to the lee of this region where the surface warm wedge first becomes evident (refer to Fig. 5). The 900 mb analysis also reveals that geostrophic flow dominates the LLJ, though a considerable ageostrophic component exists with a well-defined inflow maximum (up to 15 m s^{-1}) over the southern Appalachians.

Twelve hours later the LLJ has become less well-defined, though it still represents a (weaker) θ_e maximum within the lower troposphere. The jet axis has moved northeastward, with a 900 mb analysis (not shown) revealing 15–20 m s^{-1} winds crossing the Appalachians over West Virginia, and an ageostrophic inflow maximum over the mid-Atlantic states. A 12-h parcel trajectory within the LLJ, computed via the method of Danielsen (1961) using a correction for condensation, is sketched on Fig. 12a. The parcel starts at 900 mb at AHN at 1200 UTC 27 February and winds up at 450 mb over northern Michigan, yielding a 12-hour mean ascent rate of -10×10^{-3} mb s^{-1}.

The thermodynamic structure approximately along the LLJ axis is examined by means of θ_e cross sections in Fig. 13. The exact paths of these sections are given on Fig. 12, which shows that the 1200 UTC 27 February section passes through the snowband while the later section passes just east of the band. At 1200 UTC 27 February the frontal layer slopes gradually upward from the surface just south of AHN to about 850 mb over BNA, then ascends more steeply to nearly 700 mb at SLO. Strong frontogenesis [maximum of 1.5°C $(100\ km)^{-1}\ (3\ h)^{-1}$ from both observed wind and QG] is present within the frontal layer around SLO, and the kinematic vertical motion fields reveal a local ascent maximum of -13×10^{-3} mb s^{-1} at 700 mb on the warm side of the front just south of SLO. This position corresponds precisely with the location of the snowband. Twelve hours later the structure is similar, with a somewhat weaker increase in frontal slope between PIT and BUF. Once again this section, which is now just downstream of the snowband, exhibits strong frontogenetic forcing [maximum of 2.6°C $(100\ km)^{-1}\ (3\ h)^{-1}$ from observed winds, but only 1.1°C $(100\ km)^{-1}\ (3\ h)^{-1}$ from QG] and a kinematic ascent maximum concentrated on the warm side of the frontal zone. Finally, a growing area of potential instability, apparently responsible for the convection discussed earlier, exists just above the frontal zone. This represents the destabilizing influence of the dry intrusion overspreading the very warm moist air near the top of the frontal inversion.

A lower tropospheric vorticity analysis (not shown) reveals a cyclonic vorticity maximum of $32 \times 10^{-5}\ s^{-1}$ at 800 mb on the south side of the snowband at 1200 UTC 27 February. This maximum is embedded within an arc of large vorticity, exceeding $28 \times 10^{-5}\ s^{-1}$, that extends along the LLJ from southeastern Alabama to northern Arkansas, on the west and south sides of the kinematic ascent band (Fig. 7a). The low-level flow is characterized by very strong convergence, with the convergence term exceeding $15 \times 10^{-9}\ s^{-2}$ along the entire LLJ axis and maximizing at $25 \times 10^{-9}\ s^{-2}$ over western Kentucky, near the snowband. By 0000 UTC 28 February the vorticity at 800 mb along the LLJ has

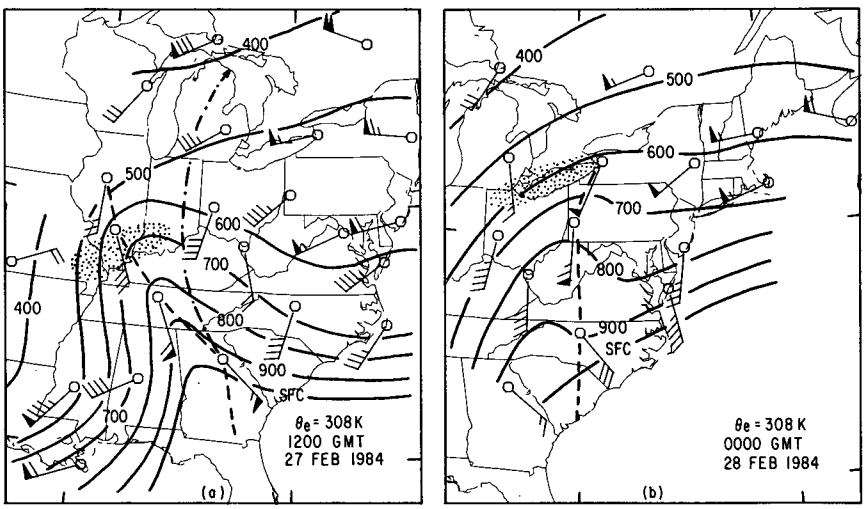

FIG. 12. Analysis of the θ_e = 308 K surface at (a) 1200 UTC 27 February 1984. (b) 0000 UTC 28 February 1984. Pressure (solid) every 100 mb, winds as in Fig. 3. Stippling marks surface snowband. Dashed lines show paths of cross-sections in Fig. 13. Dot-dashed line on panel (a) represents a 12-hour air parcel trajectory beginning at 1200 UTC 27 February.

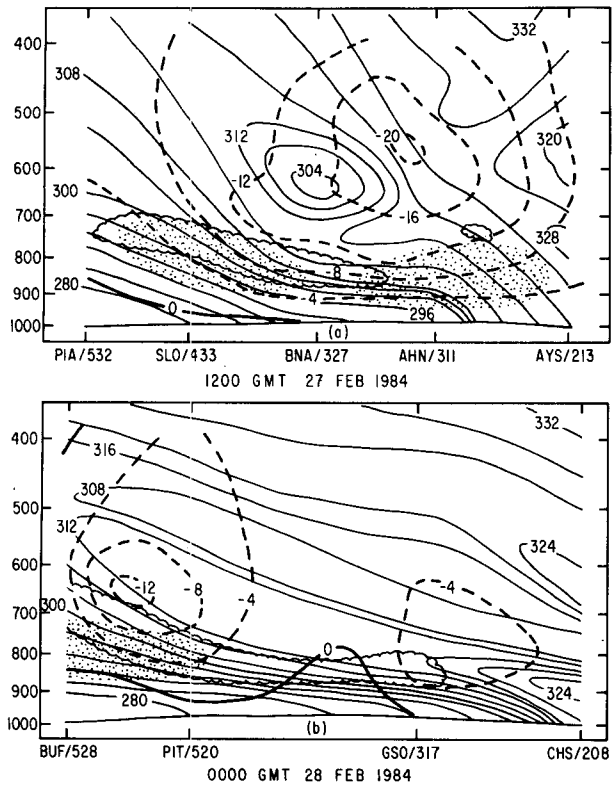

FIG. 13. Vertical cross sections along paths indicated on Fig. 12 for (a) 1200 UTC 27 February 1984 (b) 0000 UTC 28 February 1984. Thin solid lines represent equivalent potential temperature at 4 K intervals. Vertical velocity: zero contour heavy solid with ascent indicated by dashed lines, interval 4×10^{-3} mb s^{-1}. Stippling denotes regions where horizontal component of observed frontogenesis is greater than 1°C (100 km)$^{-1}$ (3 h)$^{-1}$. Scalloped line encloses the region where term 2 of equation (7) is less than -5×10^{-13} s^{-4}, i.e., where the moist potential vorticity is locally reduced.

decreased to less than 16×10^{-5} s^{-1}, apparently due to a tremendous decrease of convergence along the jet. With the convergence term now less than 10×10^{-9} s^{-2} along it, air parcels being drawn into the jet are experiencing considerably less vorticity "spinup" than occurred at earlier times. The vorticity still exceeds 28×10^{-5} s^{-1} near the snowband, where there is strong convergence (convergence term 20×10^{-9} s^{-2} over northeastern Ohio), but the largest vorticity within the lower troposphere has shifted upward to 700 mb. This vorticity increase coincides with the development of a small southwesterly jet at 700 mb, parallel to the mountains from south-central Kentucky to northeastern Ohio, with maximum winds of 25–30 m s^{-1} over east-central Ohio. This jet did not exist 12 hours earlier, so the entire development occurred between observation times. As a result, it is difficult to accurately determine the importance of the individual vorticity tendency terms, but convergence appears to have dominated.

c. *Surface*

It has been shown that the low-level warming observed west of the Appalachians coincided with where a strong LLJ crossed the mountains, suggesting that terrain-induced subsidence was significant. Figure 14 shows the orographically induced vertical velocity computed from the observed surface winds. An ascent–descent dipole straddles the mountains, with the descent being somewhat stronger. The maximum subsidence shifts northward with time, as do both the LLJ and the area of maximum surface warming. It is quite likely that the computed values are underestimates of the true maximum subsidence rate, since there are few stations near mountain-top, where the cross mountain flow is strongest.

The observed surface relative vorticity structure near the mountains is examined in Fig. 15. At 1200 UTC 27 February there is a cross mountain vorticity difference of about 8×10^{-5} s^{-1}, with a weak cyclonic vorticity maximum over southern West Virginia. Twelve hours later the cross mountain vorticity difference has nearly doubled to about 15×10^{-5} s^{-1}. This increase is the result of a slight anticyclonic vorticity increase east of the mountains, combined with a larger cyclonic vorticity increase just to the west, which has resulted in the development of an isolated, well-defined cyclonic vorticity maximum over central West Virginia. As shown earlier (Fig. 5), the surface cyclone gradually redevelops toward the local vorticity maximum over West Virginia prior to the beginning of rapid deepening.

The finding of strong terrain-induced descent underlying a region of synoptic scale ascent (compare Fig. 14 with Fig. 7), combined with the development of a surface warm air wedge and cyclonic vorticity maximum just west of the Appalachians, leads us to speculate that vortex tube stretching was an important mechanism producing cyclonic vorticity at low levels west of the mountains. In order to quantify this, a surface vorticity analysis was performed in the area of

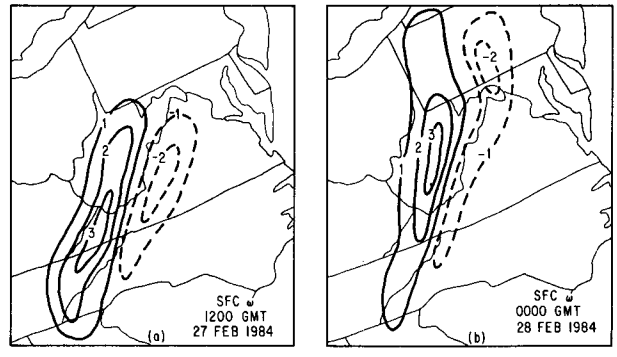

FIG. 14. Surface orographic vertical velocity (10^{-3} mb s^{-1}) for the times shown. Ascent (descent) indicated by dashed (solid) lines.

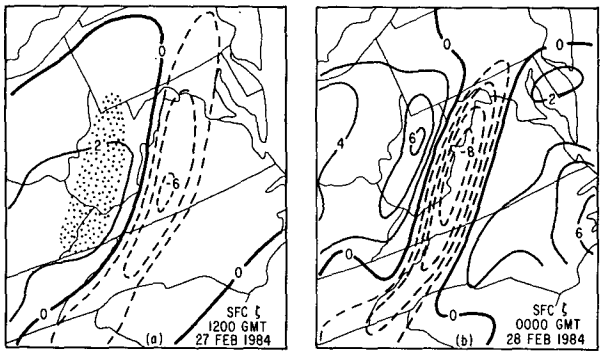

FIG. 15. Surface relative vorticity (10^{-5} s^{-1}), from observed winds, for the times shown. Zero contour heavy solid, with cyclonic (anticyclonic) relative vorticity indicated by thin solid (dashed) lines. Stippling on panel (a) indicates region of surface vorticity analysis discussed in text.

strong downslope flow from southwestern Pennsylvania to the Kentucky/Virginia border. The values of the observed vorticity, and the tendency terms in the vorticity equation, were averaged over the 7 grid point region shown on Fig. 15a, at both 1200 UTC 27 and 0000 UTC 28 February, and the results are presented in Table 1.

During the 12 hours the relative vorticity increases by approximately 80% in the lee region. Examination of the individual terms reveals that the only mechanism acting to produce vorticity is convergence, consistent with the presence of vortex tube stretching below mountain top. The combination of horizontal and vertical vorticity advection acts to offset most of the positive tendency from convergence. The result is that the predicted vorticity change, computed by averaging the total tendency for the two periods and multiplying by 12 hours, is very nearly equal to the observed vorticity change. Thus, it seems that despite their small size, the Appalachians can act as a significant source of low-level vorticity through the process of vortex tube stretching.

A computation of observed surface frontogenesis [from (5), neglecting twisting] is shown in Fig. 16. At both times strong frontogenesis is found along the southern and eastern edge of the cold air damming region, with the maxima associated with coastal frontogenesis. Elsewhere, there is little frontogenesis near the surface cold front or the snowband. A second frontogenesis maximum exists west of the Appalachians, especially at 0000 UTC 28 February. Warm air is produced locally by subsidence, then advected westward, thus strengthening the baroclinic zone parallel to and just west of the mountains. Comparison of temperature soundings from DAY and HTS (not shown) clearly reveals the effect of this frontogenesis, with considerable baroclinicity concentrated below 900 mb and little at higher levels.

5. Moist potential vorticity analysis

Bennetts and Hoskins (1979, hereafter referred to as BH) discussed the possible role of conditional symmetric instability (CSI) in the formation and maintenance of precipitation bands. This instability differs from conventional symmetric instability in that growth requires the release of latent heat of condensation, so ascending parcels must start out at or near saturation. Bennetts and Hoskins envisioned a process during which unstable air is lifted, resulting in the development of rolls oriented along the thermal wind. As the rolls grow, differential advection in the midtroposphere generates conditional gravitational instability (CGI), and the resulting convection leads to the banded nature of the precipitation. The reader interested in the details of this process is referred to Knight and Hobbs (1988), who present results of a numerical simulation of a frontal rainband that developed in a region of CSI.

According to BH, CSI is possible only if the wet-bulb potential vorticity, q_w, is negative. The wet-bulb potential vorticity is defined as

$$q_w = \left(\frac{fg}{\theta_0}\right)\boldsymbol{\eta}\cdot\nabla\theta_w$$

$$= \underbrace{\frac{g}{\theta_0} f(\zeta + f)\frac{\partial\theta_w}{\partial z}}_{\text{Term 1}} + \underbrace{\frac{fg}{\theta_0}\left(\frac{\partial u}{\partial z}\frac{\partial\theta_w}{\partial y} - \frac{\partial v}{\partial z}\frac{\partial\theta_w}{\partial x}\right)}_{\text{Term 2}}, \quad (7)$$

where $\boldsymbol{\eta}$ is the three-dimensional absolute vorticity vector, θ_w is the wet-bulb potential temperature and θ_0 is a map-averaged value of the potential temperature.

TABLE 1. Surface vorticity analysis for region shown on Fig. 15a.

Time	ω (10^{-3} mb s^{-1})	ζ (10^{-5} s^{-1})	$-(\zeta+f)\nabla\cdot\mathbf{V}$ (10^{-9} s^{-2})	$-\mathbf{V}\cdot\nabla(\zeta+f)$ (10^{-9} s^{-2})	$-\omega\frac{\partial\zeta}{\partial p}$ (10^{-9} s^{-2})	$\frac{\partial\zeta}{\partial t}$ (10^{-9} s^{-2})	$\Delta\zeta$ (predicted) (10^{-5} s^{-1})
1200 UTC 27 Feb	1.7	1.8	1.5	−0.4	−0.7	0.4	1.7
0000 UTC 28 Feb	2.1	3.1	3.1	−2.4	−0.4	0.3	1.3
	Actual $\Delta\zeta$ =	1.3				Predicted $\Delta\zeta$ =	1.5

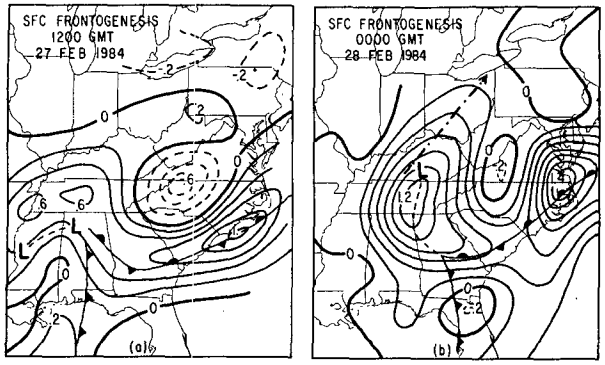

FIG. 16. Observed surface frontogenesis at (a) 1200 UTC 27 February 1984 (b) 0000 UTC 28 February 1984. Zero contour heavy solid with positive (negative) values denoted by thin solid (dashed) lines, contour interval 0.2°C (100 km)$^{-1}$ (3 h)$^{-1}$. Dashed line between low centers on (a) and extending into the low center on (b) represents position of surface trough. On (b), dot-dashed line represents position of 700 mb jet axis.

Note that terms involving the horizontal derivatives of vertical velocity have been neglected in (7). Also, note that term 1 can contribute in a negative sense if $(\zeta + f) < 0$ (inertial instability) or $\partial\theta_w/\partial z < 0$ (CGI). Since either of these instabilities will tend to dominate if present, it is necessary to examine the magnitude and sign of both $(\zeta + f)$ and $\partial\theta_w/\partial z$ before concluding that a region of $q_w < 0$ is susceptible to CSI.

The present case features a well-defined, persistent band of snow oriented along the thermal wind in a region of strong lower tropospheric baroclinicity. At times, thunderstorms were reported by stations within this band, especially those near the southern boundary (for example, see southwestern Indiana in Fig. 5b). These observations suggest that CSI may be one mechanism responsible for maintaining the snowband. Since it is important to understand and be able to predict the location and intensity of areas of banded precipitation, we have examined this possibility by computing q_w from our subjectively prepared dataset. Vertical derivatives were computed over 100 mb deep layers, and the other parameters were determined by averaging their values at the upper and lower pressure levels. Thus, for example, data from 800 and 700 mb is used to determine q_w at 750 mb. This procedure, of course, is only capable of determining the synoptic-scale structure of q_w. If there is CSI only on the scale of the band, we would not expect a clear signal due to both the vertical averaging technique used and the relatively wide separation of radiosonde stations (about 400 km).

Results (total q_w, along with term 1 and 2) for 1200 UTC 27 February are presented in Fig. 17. At 850 mb there is a large area, mainly near the Gulf coast, where q_w is negative, but in this region CGI prevails ($\partial\theta_w/\partial z < 0$, not shown). There is an elongated q_w maximum extending from southwest to northeast over the snowband. Examination of the individual terms reveals that term 1 dominates, due to the combination of strong static stability and large cyclonic vorticity within the frontal zone. However, term 2 makes a large negative contribution just south of the snowband on the warm side of the frontal zone at this level, though the contribution is generally less than one-half that of term 1.

At 750 mb q_w is still positive over the snowband, due to term 1, but the magnitude has decreased considerably from 850 mb. This reflects the much weaker values of both vorticity and stability just above (750 mb) versus within (850 mb) the frontal layer. Note that term 2 is once again offsetting term 1 on the warm side of the frontal zone, though at this level this is occurring mainly north of the surface snowband. Presumably, due to the slope of the system, at 800 mb term 2 would make a large negative contribution directly over the snowband, though probably not large enough to make $q_w < 0$. Elsewhere, there is a large region of $q_w \ll 0$ over the northern Gulf states, but this reflects CGI due to the dry intrusion above 800 mb.

The 0000 UTC 28 February results are not shown because the patterns, though shifted northeastward, are identical to those of 12 hours earlier. However, the magnitude of all terms has increased, reflecting the intensification of the lower tropospheric baroclinic zone during the period. Once again, term 2 acts as a significant source of negative q_w on the warm side of the baroclinic zone. Also, it should be mentioned that at both times the moist potential vorticity above 750 mb decreased upward near the snowband, approaching 0 at 550 mb, well above the level of maximum ascent within the band (see Fig. 13). Finally, for comparison q_w (7) was recomputed using the geostrophic wind. This resulted in no change of the spatial structure of the features in Fig. 17. However, q_w was increased by as much as 20×10^{-13} s^{-4} at 850 mb within the q_w maximum near the snowband, due to the geostrophic vorticity being larger than observed. Elsewhere, changes in the value of q_w were generally small (less than 5×10^{-13} s^{-4}), indicating the domination of the geostrophic flow component, even within the LLJ (and in the snowband above 850 mb).

The evidence presented suggests that CSI is not the mechanism responsible for maintenance of the snowband, since there are no negative q_w values directly associated with it. However, there is a persistent area on the warm side of the baroclinic zone near the snowband where term 2 is large negative, and thus locally reduces the moist potential vorticity. Although in this case term 2 is not large enough to make $q_w < 0$, it could do so in other situations. Therefore, it is worthwhile to determine why term 2 is contributing in the negative sense in the aforementioned areas.

Recall from earlier results that a LLJ, associated with a local θ_w maximum, ascended the baroclinic zone just east of the snowband (for example, see Fig. 12). A schematic cross section, taken perpendicular to the jet from west to east, is presented in Fig. 18 (refer to Fig. 17f for representative location of this section). The

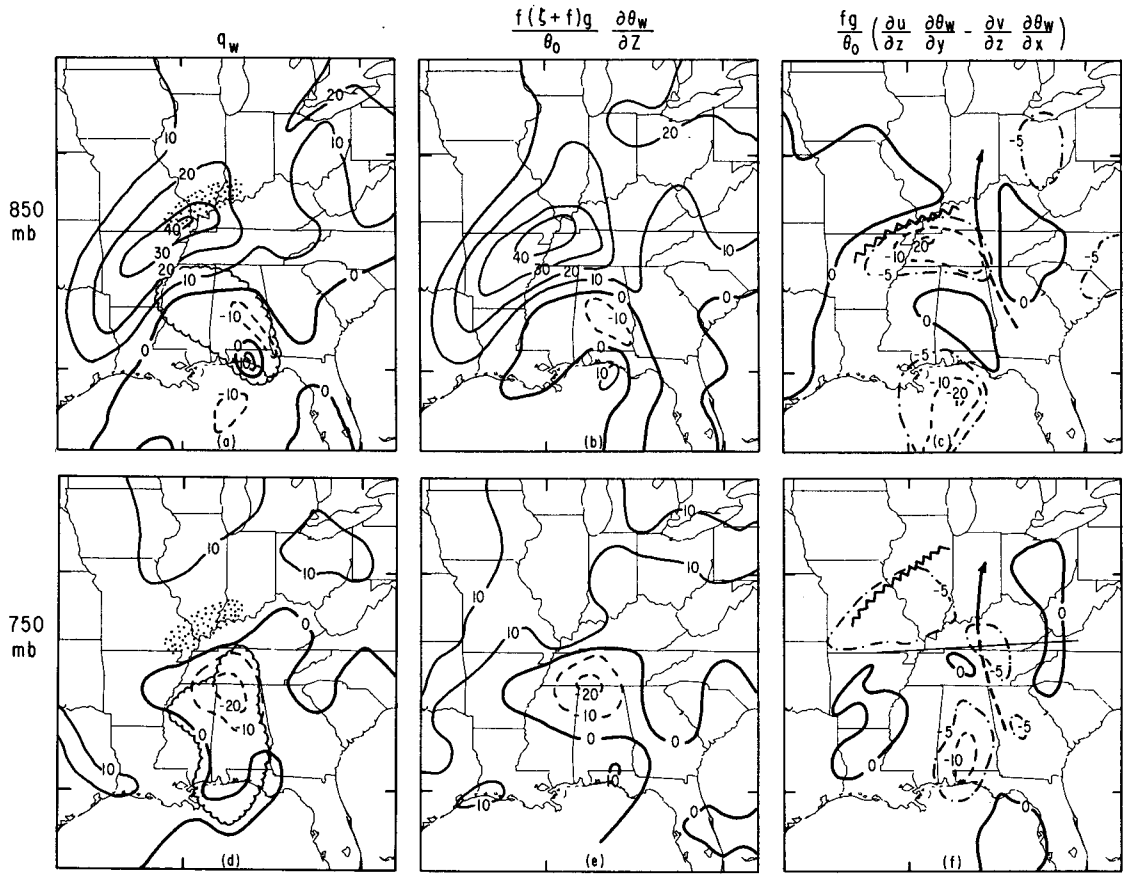

FIG. 17. Moist potential vorticity analysis at 1200 UTC 27 February 1984 for 850 mb (top) and 750 mb (bottom). (a), (d) Total moist potential vorticity. (b), (e) Term 1 of Eq. (7). (c), (f) Term 2 of Eq. (7). Zero contour heavy solid, with positive (negative) values denoted by medium solid (dashed) lines. Contour interval 10×10^{-13} s^{-4}, except on (c) and (f), where -5×10^{-13} s^{-4} contour has been added (dot-dashed). Stippling (panels a, d) marks surface snowband. Zig-zag line (panels c and f) marks position of frontal boundary. On (c) and (f), line with arrow represents low-level jet, solid (dashed) part is above (below) the particular pressure surface. On (a) and (d) scalloped lines enclose regions where $dq_w/dt < -5 \times 10^{-18}$ s^{-5}. On (f), thin solid approximately east–west line is path of schematic cross section in Fig. 18.

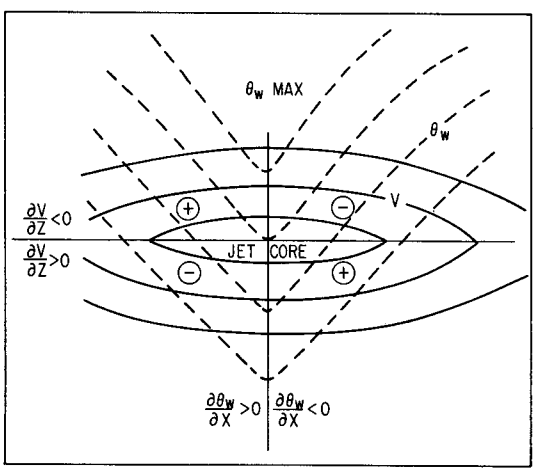

FIG. 18. Schematic vertical cross section from west (left) to east (right) through low-level jet showing sign of terms in equation (8). Isotachs are solid, θ_w lines are dashed. Vertical coordinate is height, increasing upward.

flow is into the page, and if we align the y-axis along the jet, term 2 becomes

$$q_w = -\frac{fg}{\theta_0}\frac{\partial v}{\partial z}\frac{\partial \theta_w}{\partial x}. \tag{8}$$

The sign of this term is indicated on Fig. 18, which shows the existence of a 4-cell pattern centered about the LLJ, with two regions of reduced q_w—one above and to the right of the jet and one below and to the left. Reference to Fig. 17 reveals that the reduced q_w region on the warm side of the baroclinic zone, over western Tennessee at 850 mb and southern Illinois and Missouri at 750 mb, coincides with the lower left "box." Thus, the presence of a strong LLJ associated with a local θ_w maximum results in regions of reduced q_w that could become susceptible to CSI if the magnitude of term 2 becomes large enough. [Note: the area where term 2 is negative over southern Alabama in Fig. 17f is actually in the upper left box with respect to the LLJ,

in apparent violation of Fig. 18. However, this reflects a complex interaction between the base of the upper-level southwesterly jet (see Fig. 4b) and the dry slot (see Fig. 6a) at 700 mb, and the LLJ below, and thus should not be interpreted as being solely related to the LLJ].

6. Discussion

a. Moist potential vorticity

The moist potential vorticity analysis of the preceding section failed to reveal any evidence for CSI as the maintenance mechanism for the snowband. However, there was a zone of locally reduced moist potential vorticity on the warm side of the lower tropospheric baroclinic zone near the snowband, due to the presence of a strong LLJ embedded within a local θ_w maximum. Thus, we have a frontal zone with an effective potential vorticity gradient such that the warm air has relatively low potential vorticity compared to the cold air. Emanuel (1985) and Emanuel et al. (1987) theoretically studied the vertical circulation that develops when such a region is subjected to frontogenetic forcing. They found that an asymmetric circulation develops, with strong sloping ascent concentrated on the warm side of the front and widespread weaker descent in the cold air. Examination of the cross sections through the snowband (Fig. 13) reveals that the ascent maximizes in a sloping region on the warm air side (i.e., reduced moist potential vorticity zone) of a baroclinic zone being subjected to strong frontogenetic forcing, in qualitative agreement with the findings of Emanuel. Similar results were obtained by Sanders and Bosart (1985) in their study of an east coast snowstorm, though they used a different approach to determine the degree of CSI present.

Our results suggest that analysis of the q_w field within the lower troposphere could be a useful tool for forecasting the formation and maintenance of precipitation bands in the frontogenetic regions of lower tropospheric baroclinic zones. However, to be really useful, q_w would have to be computed from a carefully analyzed dataset with good horizontal (at least 1° latitude–longitude) and vertical (at least 100 mb) resolution. At present, the initial analysis and/or resulting forecast fields from a sufficiently high resolution numerical model, such as the RAFS (Phillips 1979; DiMego 1988) may be the best available dataset for this computation. In fact, Bennetts and Sharp (1982) performed such a study using numerical model output. They evaluated the magnitude of a growth rate parameter σ^2, defined as

$$\sigma^2 = -q_w \Big/ \left(\frac{g}{\theta_0} \frac{\partial \theta_w}{\partial z} \right). \tag{9}$$

If $\partial\theta_w/\partial z > 0$ (gravitational stability), then there is CSI if $\sigma^2 > 0$, which is the same as requiring $q_w < 0$. Despite using a vertical layer 150 mb deep for their calculations, their results showed that where $\sigma^2 > 0$ there was generally banded precipitation, with the likelihood increasing as the magnitude of σ^2 increased. They did not, however, examine the actual magnitude of q_w or its components individually.

An important unresolved issue involves the mechanism by which negative moist potential vorticity is produced within a cyclone. Bennetts and Hoskins derived a moist potential vorticity tendency equation as

$$\frac{dq_w}{dt} = f \frac{g^2}{{\theta_0}^2} \mathbf{k} \cdot (\nabla \theta_\omega \times \nabla \theta) + f \frac{g}{\theta_0} \vec{\eta} \cdot \nabla Q + f \frac{g}{\theta_0} \mathbf{F} \cdot \nabla \theta_\omega, \tag{10}$$

where Q represents diabatic effects and $\mathbf{F}$ is a frictional term. Computation of frictional and diabatic effects was beyond the scope of this work, but we did evaluate the first term on the right side of (10). In general, this term was of the order $\sim \pm 10 \times 10^{-18}$ s^{-5}, which corresponds to a q_w change of $\sim \pm 8 \times 10^{-13}$ s^{-4} day^{-1}. Regions where this term was important in decreasing q_w (i.e., dq_w/dt less than -5×10^{-18} s^{-5}) are marked on panels (a) and (d) of Fig. 17. These areas, with a minimum dq_w/dt of -37×10^{-18} s^{-5}, are located within the dry intrusion south of the snowband, where q_w is generally already negative (or nearly so). Along the leading (northward) edge of the negative moist potential vorticity region, where q_w is less than 10×10^{-13} s^{-4}, the time scale for producing negative q_w ranges from 3 to 15 hours in the layer from 850–650 mb. Physically, this term reflects the differential advection of dry, low θ_w air over moist, higher θ_w air at the top of the frontal inversion, which increases the susceptibility of the atmosphere to CSI by decreasing the vertical stability. In this case, however, the destabilization is so strong that CGI results, aiding the development of convection near the cyclone center prior to rapid deepening.

In order to get some idea of the possible importance of the remaining terms in (10), we performed a scale analysis based upon conditions representative of the snowband environment. For the diabatic term, we used a precipitation rate of 10 mm (6 h)$^{-1}$, with the resultant latent heat distributed between 850 and 450 mb. With $\zeta = 18 \times 10^{-5}$ s^{-1} and $\theta_0 = 273$ K, we obtain for dq_w/dt a value of $\pm 50 \times 10^{-18}$ s^{-5}, similar in magnitude but numerically larger than any values actually computed from the first term. The diabatic term would act to decrease (increase) q_w above (below) the level of maximum heating, and thus could be, at least partially, responsible for the observed vertical structure of q_w near the band, i.e., very large at 850 mb below the level of maximum ascent ($\sim$700 mb) and nearly zero above it at 550 mb. At 650 mb, just above the ascent maximum, the time scale to produce negative q_w would be 3–4 hours. In this case, the diabatic term would be most important near the snowband several hundred

kilometers north of where the first term was important, but it could also be large near the area of convection embedded within the dry intrusion south of the snowband.

Finally, the friction term was estimated using an eddy viscosity coefficient of 5 $m^2 s^{-1}$, a vertical wind shear of 10 m s^{-1}/km and a vertical θ_w gradient of 2°C km^{-1}. This yields 0.7×10^{-18} s^{-5} for dq_w/dt, corresponding to a moist potential vorticity change of 0.6×10^{-13} s^{-4} day^{-1}. Thus, it seems that frictional effects are significantly smaller than the other terms in (10).

b. *Influence of mesoscale precipitation systems on the synoptic scale*

An intriguing aspect of this study was the decoupling that occurred between the midtropospheric short-wave trough and the surface cyclone. The 1200 UTC 27 February QG analysis (Fig. 8b) showed a region of very strong forcing of ascent at 500 mb well north of the surface low. LFM initial vorticity analyses (not shown) reveal that this area of forcing was associated with the short-wave trough responsible for the original development of the cyclone as it moved away from the Rockies. The decoupling process occurred while two mesoscale precipitation features, the snowband and squall line, were intensifying on either side of the low. At 1200 UTC 27 February both features were dominated by lower tropospheric forcing, which resulted in strong ascent maxima below 600 mb. This is documented in Fig. 19, which shows vertical profiles of the vertical velocity and horizontal divergence within the snowband and squall line, and the region between. These values represent an average over six grid points within each feature. Ascent maximizes at about 650 mb in both the snowband and squall line, and divergence is present in the 600–400 mb layer above both features. This divergence of air aloft from the snowband and squall line forces a region of midtropospheric convergence between them, as seen from Fig. 19, which acts to suppress low and midtropospheric ascent between the precipitation systems.

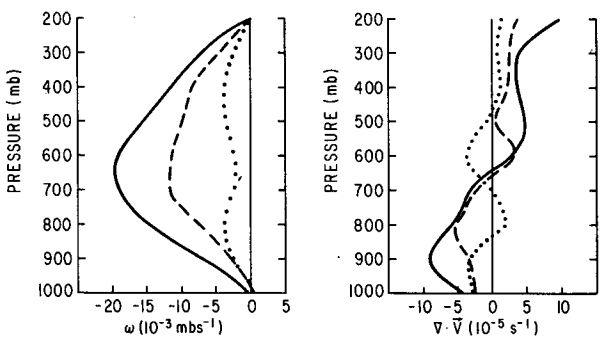

FIG. 19. Vertical profiles of kinematic vertical velocity (left, 10^{-3} mb s^{-1}) and horizontal divergence (right, 10^{-5} s^{-1}) for the squall line (solid), snowband (dashed) and the region between (dotted) at 1200 UTC 27 February 1984.

The cyclone first began to exhibit signs of weakening around 0000 UTC 27 February, and the synoptic situation at this time is depicted schematically in Fig. 20. The squall line is intensifying southeast of the cyclone while the snowband is becoming organized on an axis from extreme northern Texas to southwestern Missouri. We speculate, based on the vertical profiles of divergence and ω at 1200 UTC 27 February, that the synoptic-scale divergence field associated with CVA is locally overwhelmed by the superimposed mesoscale convergence field associated with the precipitation systems. This eliminates surface pressure falls in the vicinity of the low center, which is situated between the precipitation systems, so that as the short-wave turns northeastward into the Mississippi Valley, the surface low fails to do so.

Of course, this scenario is highly dependent upon the questionable assumption that the vertical profiles of ω and divergence are the same at both 0000 and 1200 UTC 27 February. In order to test the validity of this assumption, we subjectively analyzed the wind field at 850, 500 and 300 mb for a 15° × 15° region centered on the cyclone at 0000 UTC 27 February, and computed the divergence, vorticity and horizontal vorticity advection. The results, superimposed on Fig. 20, lend credence to our hypothesis. Strong cyclonic vorticity advection is present over and just upstream of the low. Quasi-geostrophic theory indicates that such a region should exhibit midtropospheric divergence which causes surface pressure falls, i.e., the cyclone should deepen. However, two areas of strong low-level convergence, associated with the squall line and developing snowband, straddle the cyclone. Divergence at 500 mb above these features (not shown) forces a band of midtropospheric convergence from southwestern Missouri to eastern Texas, passing directly over the cyclone center. Thus, it seems that the intensification of two mesoscale precipitation systems on either side of the cyclone center creates an intense ageostrophic circulation which forces midtropospheric convergence over the low. This appears to disrupt the synoptic scale circulation, causing the decoupling of the surface low and the midtropospheric short-wave trough.

c. *Influence of topography*

After the decoupling took place, the surface cyclone tracked eastward across the Gulf states, then turned northeastward as the midtropospheric flow became increasingly southwesterly. The original vortex dissipated over west-central Kentucky while a series of new circulation centers developed further east in the warm air wedge along the western side of the Appalachians. This was a region of considerable terrain induced subsidence, caused by the crossing of the mountains by a well-developed southeasterly low-level jet. Large scale

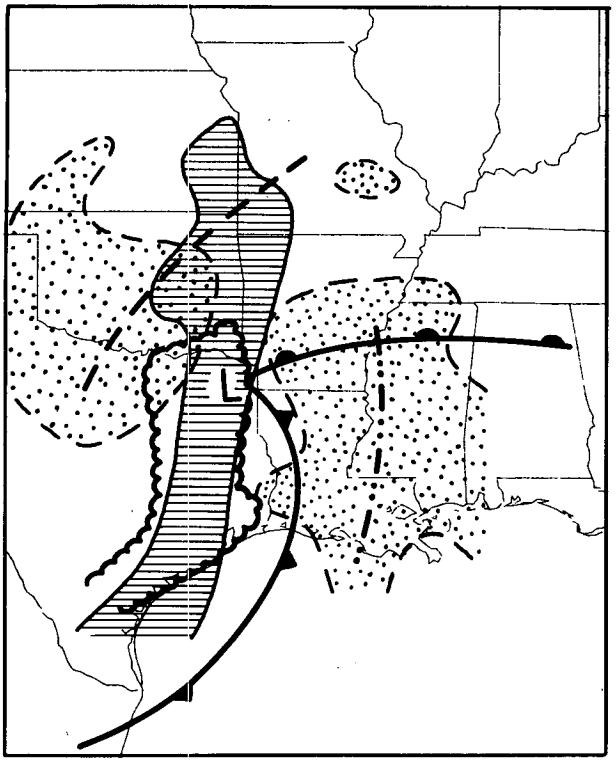

FIG. 20. Surface schematic for 0000 UTC 27 February 1984. Snowband and squall line denoted by dashed and dot-dashed lines, respectively. Stippled area denotes where 850 mb convergence exceeds -2×10^{-5} s^{-1}, hatched area where 500 mb convergence exceeds -2×10^{-5} s^{-1}. Scalloped line encloses the area where the 500 mb horizontal cyclonic vorticity advection exceeds 5×10^{-9} s^{-2}.

ascent in this jet, combined with the low-level subsidence west of the mountains, resulted in the production of cyclonic vorticity below mountaintop, in a band from eastern Kentucky to southwestern Pennsylvania, through the vortex tube stretching mechanism. This produced a local maximum of cyclonic vorticity over central West Virginia, and the surface low slowly redeveloped toward this region prior to deepening.

In addition to acting as a low-level vorticity source, the Appalachians altered the thermodynamic structure of the atmosphere through a fairly deep layer. The production of warm air by orographic subsidence created a lower tropospheric baroclinic zone west of the mountains (see Fig. 16), marked by a local maximum in the 1000–700 mb thickness field (not shown). We speculate that the development of a 700 mb jet along the western edge of this baroclinic zone represents the result of a geostrophic adjustment process (Rossby 1938) to the increasing thermal gradient, particularly since the vertical wind shear over Ohio was approximately in thermal wind balance (not shown). This jet appears to merge with the LLJ crossing the mountains from the southeast (Fig. 12b), resulting in a local enhancement of the wind speed over eastern Ohio and western Pennsylvania. The associated increase in vertical wind shear acts to decrease the moist potential vorticity, thus aiding the maintenance of the snowband.

d. Possible role of the upper-level front in cyclogenesis

The final deepening phase of the cyclone began around 0600 UTC 28 February as an intense upper-level frontal zone moved over the Appalachians. As this frontal zone entered the large-scale confluent, frontogenetic southwesterly flow ahead of the long-wave trough, there was considerable cyclonic vorticity production by convergence. This vorticity was advected downstream in a narrow band, resulting in two areas of enhanced midtropospheric cyclonic vorticity advection. Interpolation revealed that the cyclone began deepening when the second area of vorticity advection overspread the vorticity rich lower troposphere over West Virginia.

In a thorough review of the structure and dynamics of upper-level frontal zones, Keyser and Shapiro (1986) briefly addressed the issue of whether such fronts play an active or passive role in surface cyclogenesis. While certainly not conclusive, the evidence presented here suggests that upper-level fronts may, at least in some cases, act to focus, if not initiate, surface cyclogenesis. Our detailed subjective analysis revealed the existence of a narrow band of cyclonic vorticity associated with the upper front at 0000 UTC 28 February (Fig. 11a). Comparison with the LFM model initial vorticity analysis (Fig. 21) reveals that the model was not able

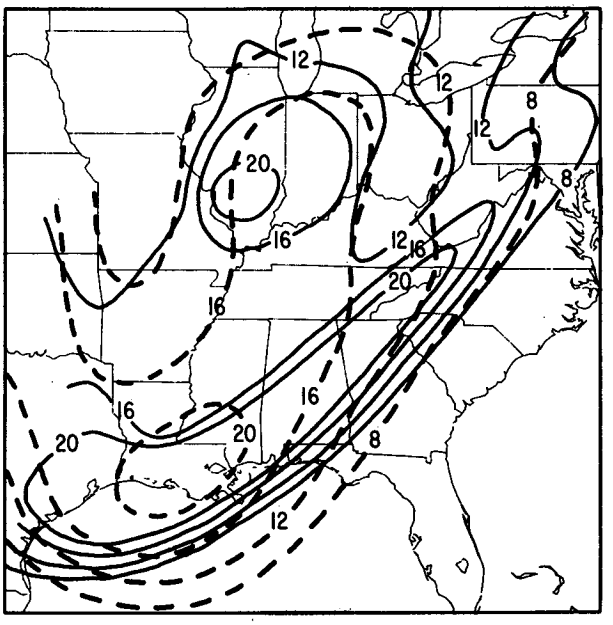

FIG. 21. The 500 mb absolute vorticity (10^{-5} s^{-1}) at 0000 UTC 28 February 1984. LFM model analysis (dashed) versus our subjective analysis (solid). Contour interval 4×10^{-5} s^{-1}. For clarity, the 24 and 28 contours of the subjectively analyzed vorticity have been omitted.

to accurately reproduce this small scale feature. Instead, the vorticity was spread out over a larger area, resulting in weak vorticity gradients. This in turn caused the model cyclonic vorticity advection to be too weak and unfocused compared to the real atmosphere. It is possible that this was a major cause of the model's inability to simulate the rapidity of the deepening that took place after 0600 UTC 28 February—the model forecast initialized at 0000 UTC 28 February predicted a central pressure of 995 mb after 12 hours, while 990 mb was observed. Other factors undoubtedly played a role, including the lower tropospheric thermal and vorticity structure west of the mountains. A typical error in the LFM model forecasts initialized before 0000 UTC 28 February was that the cyclone center was too far west of the mountains, by 150–250 km. This suggests that the model was not able to properly simulate the localized production of cyclonic vorticity occurring near the surface west of the Appalachians. Thus, both the lower and midtropospheric vorticity fields in the model were too weak, resulting in a slower development than actually took place. It is possible that knowledge of the location and intensity of upper-level frontal zones could help one improve the timing and rapidity of numerical model surface cyclogenesis forecasts in at least some cases.

7. Conclusions

This paper presents an analysis of a cyclone which affected most of the eastern half of the United States in late February 1984. The cyclone developed through the typical lee cyclogenesis process (i.e., Hess and Wagner 1948; McClain 1960) when a midtropospheric short-wave trough crossed the southern Rockies. Upon reaching eastern Texas, however, the surface cyclone became separated, or decoupled, from the short-wave trough, resulting in the weakening and disorganization of the low-level circulation. The cyclone subsequently redeveloped toward the Appalachian mountains, then underwent a second period of intensification, which coincided with the arrival of a strong upper-tropospheric frontal zone over the surface cyclone.

During most of its life, the cyclone was accompanied by a persistent, mesoscale band of heavy snow located approximately 500 km north-northwest of the center. This snowband was oriented along an intensifying lower-tropospheric baroclinic zone. Examination of the moist potential vorticity structure (Bennetts and Hoskins 1979) suggested that conditional symmetric instability was not the maintenance mechanism. However, a sloping region of reduced moist potential vorticity was found on the warm side of the baroclinic zone, due to the presence of an ascending low-level jet embedded within a θ_w maximum. Ascent within the snowband was concentrated on the warm side of the baroclinic zone, suggesting that the intensity of the band was the result of an enhancement of a frontogenetic circulation by a potential vorticity gradient, as discussed theoretically by Emanuel (1985) and Emanuel et al. (1987).

The decoupling of the cyclone from the midtropospheric short-wave trough appeared to be caused by the simultaneous intensification of two mesoscale precipitation systems on either side of the cyclone. Both the snowband to the northwest and a squall line to the southeast were characterized by strong lower tropospheric convergence, which led to ascent maxima in the 650–700 mb layer. Divergence above these systems in the 600–500 mb layer forced a band of midtropospheric convergence between them. This convergence, which was located directly over the cyclone when the decoupling began, was apparently sufficient to overwhelm midtropospheric divergence forced by differential cyclonic vorticity advection, leading to the observed decoupling.

After becoming decoupled from the short-wave trough, the cyclone redeveloped toward the Appalachian mountains in response to low-level vorticity generation west of the mountains. This vorticity was produced by vortex tube stretching, due to terrain-induced subsidence where a strong southeasterly low-level jet crossed the mountains.

The final deepening of the cyclone occurred when a strong upper-level front moved over the Appalachians from the southwest. This front was associated with a narrow band of large cyclonic vorticity produced by convergence in the confluent southwesterly flow ahead of the longwave trough. As this vorticity was advected over the lower tropospheric vorticity maximum west of the mountains, rapid surface intensification took place. An active role for upper-level frontal zones in surface cyclogenesis is indicated.

Acknowledgments. The computational assistance of Dr. Chung-Chieng Lai is very much appreciated. The National Center for Atmospheric Research provided most of the observations. Marilyn Peacock drafted the figures while Celeste Iovinella prepared the manuscript. The research was supported by National Science Foundation Grant ATM-8311106.

REFERENCES

Bell, G. D., and L. F. Bosart, 1988: Appalachian cold air damming. *Mon. Wea. Rev.*, **116**, 137–161.

Bennetts, D. A., and B. J. Hoskins, 1979: Conditional symmetric instability—a possible explanation for frontal rainbands. *Quart. J. Roy. Meteor. Soc.*, **105**, 945–962.

——, and J. C. Sharp, 1982: The relevance of conditional symmetric instability to the prediction of mesoscale frontal rainbands. *Quart. J. Roy. Meteor. Soc.*, **108**, 595–602.

Bosart, L. F., 1975: New England coastal frontogenesis. *Quart. J. Roy. Meteor. Soc.*, **101**, 957–978.

——, and A. Seimon, 1988: A case study of an unusually intense atmospheric gravity wave. *Mon. Wea. Rev.*, **116**, 1857–1886.

Carr, F. H., and J. P. Millard, 1985: A composite study of comma clouds and their association with severe weather over the Great Plains. *Mon. Wea. Rev.*, **113**, 370–387.

Dallavalle, J. P., and L. F. Bosart, 1975: A synoptic investigation of

anticyclogenesis accompanying North American polar air outbreaks. *Mon. Wea. Rev.*, **103,** 941–957.

Danielsen, E. F., 1961: Trajectories: Isobaric, isentropic and actual. *J. Meteor.*, **3,** 479–486.

DiMego, G. J., 1988: The National Meteorological Center Regional Analysis System. *Mon. Wea. Rev.*, **116,** 977–1000.

Durran, D. R., and L. W. Snellman, 1987: The diagnosis of synoptic-scale vertical motion in an operational environment. *Wea. Forecasting,* **2,** 17–31.

Emanuel, K. A., 1985: Frontogenesis in the presence of low moist symmetric stability. *J. Atmos. Sci.*, **42,** 1062–1072.

——, M. Fantini and A. J. Thorpe, 1987: Baroclinic instability in an environment of small stability to slantwise moist convection. Part I: Two-dimensional models. *J. Atmos. Sci.*, **44,** 1559–1573.

Forbes, G. S., R. A. Anthes and D. W. Thomson, 1987: Synoptic and mesoscale aspects of an Appalachian ice storm associated with cold-air damming. *Mon. Wea. Rev.*, **115,** 564–591.

Gerrity, J. F., 1977: The LFM model—1976: A documentation. NOAA Tech. Memo. NWS NMC-60 (NTIS no. PB-279-419.)

Hane, C. E., 1986: Extratropical squall lines and rainbands. *Mesoscale Meteorology and Forecasting,* P. S. Ray, Ed., Amer. Meteor. Soc., Chapter 16.

Hess, S. L., and H. Wagner, 1948: Atmospheric waves in the northwestern United States. *J. Meteor.*, **5,** 1–19.

Hoskins, B. J., and M. A. Pedder, 1980: The diagnosis of middle latitude synoptic development. *Quart. J. Roy. Meteor. Soc.*, **106,** 707–719.

——, I. D. Draghici and H. C. Davies, 1978: A new look at the omega equation. *Quart. J. Roy. Meteor. Soc.*, **104,** 31–38.

Keyser, D., 1986: Atmospheric Fronts: An observational perspective. *Mesoscale Meteorology and Forecasting,* P. S. Ray, Ed., Amer. Meteor. Soc., Chapter 10.

——, and M. A. Shapiro, 1986: A review of the structure and dynamics of upper-level frontal zones. *Mon. Wea. Rev.*, **114,** 453–499.

Knight, D. J., and P. V. Hobbs, 1988: The mesoscale and microscale structure and organization of clouds and precipitation in midlatitude cyclones. Part XV: A numerical modeling study of frontogenesis and cold-frontal rainbands. *J. Atmos. Sci.*, **45,** 915–930.

McClain, E. P., 1960: Some effects of the Western Cordillera of North America on cyclone activity. *J. Meteor.*, **17,** 104–115.

Miller, J. E., 1948: On the concept of frontogenesis. *J. Meteor.*, **5,** 169–171.

O'Brien, J. J., 1970: Alternative solutions to the classical vertical velocity problem. *J. Meteor.*, **9,** 197–203.

Phillips, N. A., 1979: The Nested Grid Model. NOAA Tech. Rep. NWS22, 80 pp. [Available from Environmental Science Information Center (D822), NOAA, Rockville, MD., 20852.]

Richwein, B. A., 1980: The damming effect of the southern Appalachians. *Natl. Wea. Dig.*, **5,** 2–12.

Rossby, C. G., 1938: On the mutual adjustment of pressure and velocity distributions in certain simple current systems. II. *J. Mar. Res.*, **7,** 239–263.

Sanders, F., 1955: An investigation of the structure and dynamics of an intense surface frontal zone. *J. Meteor.*, **12,** 542–552.

——, and L. F. Bosart, 1985: Mesoscale structure in the Megalopolitan snowstorm of 11–12 February 1983. Part I: Frontogenetical forcing and symmetric instability. *J. Atmos. Sci.*, **42,** 1050–1061.

Uccellini, L. W., and D. R. Johnson, 1979: The coupling of upper and lower tropospheric jet streaks and implications for the development of severe convective storms. *Mon. Wea. Rev.*, **107,** 682–703.